



1th International
WHEEL
seminar

5th International
Geoscience
Symposium



Precambrian World 2023

Earth through History

Kochi core center, Japan

March 5 (Sun) - 6 (Mon) 2023

Field trip: March 7-10



<http://wheelaa.jp>

Okitsu Melange
Kochi, Japan

*--Modern, Past and Future of Earth
Recorded: geologic, oceanic, biogenic
evidences during 4.6Ga--*

Your Name:

Welcome

The organizing committees are delighted to welcome all of you to the **5th International Geoscience Symposium “ Precambrian World 2023”** jointed with the **Whole history of Earth environmental change recorded location (WHEEL)** project seminar to be held at the Center for Advanced Marine Core Research, Kochi University in Nankoku-city, Kochi, Japan. The WHEEL project is a gathering to encourage international research (especially clarification of earth history, tectonics and environmental change research) conducted with many universities and research institutes based in Kyushu University. This symposium supported by Kyushu University, JSPS Core-to-Core program, Kochi University/JAMSTEC, Marine Core (地球掘削科学国際研究拠点 (JURC-DES) 研究集会), Ibaraki University, National Institute of Polar Research, National Museum of Nature and Science, Tokyo, Geological Survey of Japan and Japanese Society for Geocollege. We are having a truly international gathering and the joint forum between Precambrian and modern earth sciences.

Since the 1st IGS “Precambrian World 2009” and 4th IGS “Precambrian World 2017”, several natural hazards and COVID occurred in world. The earth is undergoing not only environmental changes, but also changes in culture, national and human relationships. We still need international cooperation to overcome the closed small world.

For that reason, we planned a symposium to recreate a society where researchers and young people can interact more and more.

The purpose of this symposium is to bring together international expert to discuss recent progress related to Iron formation, hydrothermal systems, microbial activity, Snowball earth system, meteorite impact, volcanic activity and great oxidation events throughout the Earth’s history. Understand of evolution for the hydrothermal systems in early Earth condition has direct implications for the evolution of atmosphere and life evolution. Recent technological developments have more opened up several new sciences and result. We do share such excitements in this symposium.

In this symposium, we will try to interact with people from all over the world, break away from the era that was closed due to the COVID, and once again support the international activities of young people.

The Organizing committees will make every effort to provide excellent environments for comfortable and enjoyable scientific gathering. We hope you enjoy your Kochi and Shikoku Island.

Organizing committee of 5th IGS “Precambrian World 2023”
and the 1st WHEEL project team



WEHHL Member

Leader Shoichi Kiyokawa, Kyushu Univ.

Takashi Ito, Ibaraki Univ.

Minoru Ikehara, Kochi Univ.

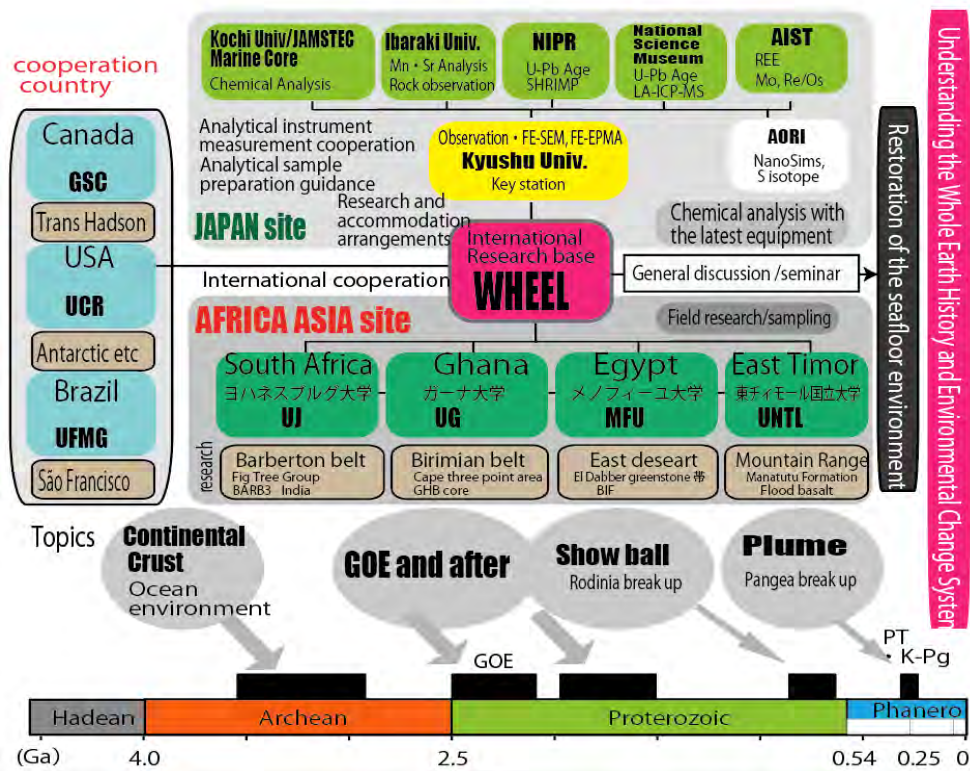
Kosuke Goto, Geological Survey of Japan (AIST)

Kenji Horie, National Polar Inst.

Mami Takehara, National Polar Inst.

Yukiyasu Tsutsumi, National museum of Nature and Science, Tokyo

Overview of the WHEEL project diagram



JAPAN SOCIETY FOR THE PROMOTION OF SCIENCE
日本学術振興会



研究拠点形成事業

Location and Accesses



高知大学海洋コア総合研究センター

Center for Advanced Marine Core Research, Kochi University

〒783-8502 南国市物部乙 200 / 200 Monobe-otsu Nankoku city Kochi, Japan

海洋コア総合研究センター事務室 / Center for Advanced Marine Core Research

TEL : 088-864-6712

FAX : 088-864-6713

E-mail : kk21@kochi-u.ac.jp

高知龍馬空港
Kochi Ryoma Airport

⑥番のりば

JR高知駅発(東部自動車道経由) → 高知龍馬空港行

	JR 高知駅 JR Kochi Station	高知駅前 Kochi ekimae	高知橋 Kochi bashi	蓮池町通 Hasuake machiuchi	北はりまや 橋 Kita Harimayaba bashi	はりまや橋 Harimaya bashi	菜園橋 Saenba	宝永町 Hoei cho	知聖町 二丁目 Chiyori cho Nishome	⇄	高知 龍馬空港 Kochi Ryoma Airport
1便	6:30	6:31	6:32	6:32	6:33	6:35	6:36	6:37	6:38		7:00
3便	6:50	6:51	6:52	6:52	6:53	6:55	6:56	6:57	6:58		7:20
5便	7:30	7:31	7:32	7:32	7:33	7:35	7:36	7:37	7:38		8:07
7便	7:50	7:51	7:52	7:52	7:53	7:55	7:56	7:57	7:58		8:27
9便	8:10	8:11	8:12	8:12	8:13	8:15	8:16	8:17	8:18		8:45
11便	8:30	8:31	8:32	8:32	8:33	8:35	8:36	8:37	8:38		9:04
13便	8:50	8:51	8:52	8:52	8:53	8:55	8:56	8:57	8:58		9:22
16便	9:10	9:11	9:12	9:12	9:13	9:15	9:16	9:17	9:18		9:42
17便	10:10	10:11	10:12	10:12	10:13	10:15	10:16	10:17	10:18		10:43
19便	10:30	10:31	10:32	10:32	10:33	10:35	10:36	10:37	10:38		11:01
21便	10:50	10:51	10:52	10:52	10:53	10:55	10:56	10:57	10:58		11:21
23便	11:10	11:11	11:12	11:12	11:13	11:15	11:16	11:17	11:18		11:41
25便	12:10	12:11	12:12	12:12	12:13	12:15	12:16	12:17	12:18		12:41
27便	12:30	12:31	12:32	12:32	12:33	12:35	12:36	12:37	12:38		13:02
29便	12:50	12:51	12:52	12:52	12:53	12:55	12:56	12:57	12:58		13:24
31便	13:10	13:11	13:12	13:12	13:13	13:15	13:16	13:17	13:18		13:42
33便	13:30	13:31	13:32	13:32	13:33	13:35	13:36	13:37	13:38		14:02
35便	14:10	14:11	14:12	14:12	14:13	14:15	14:16	14:17	14:18		14:42
37便	14:30	14:31	14:32	14:32	14:33	14:35	14:36	14:37	14:38		15:03
39便	15:10	15:11	15:12	15:12	15:13	15:15	15:16	15:17	15:18		15:40
41便	15:30	15:31	15:32	15:32	15:33	15:35	15:36	15:37	15:38		16:03
43便	15:50	15:51	15:52	15:52	15:53	15:55	15:56	15:57	15:58		16:23
45便	16:50	16:51	16:52	16:52	16:53	16:55	16:56	16:57	16:58		17:23
47便	17:30	17:31	17:32	17:32	17:33	17:35	17:36	17:37	17:38		18:05
49便	17:50	17:51	17:52	17:52	17:53	17:55	17:56	17:57	17:58		18:25
51便	18:10	18:11	18:12	18:12	18:13	18:15	18:16	18:17	18:18		18:45

高速道路(東部自動車道)経由にて運行

Kochi station to Airport

JR Kochi Station No 6 gateway

空港連絡バス時刻表
Airport Limousine Bus Schedule

令和4年12月1日

バスのりば

高知龍馬空港発(東部自動車道経由) → JR高知駅行

	高知 龍馬空港 Kochi Ryoma Airport	⇄	知聖町 Chiyori cho	宝永町 Hoei cho	菜園橋 Saenba	北はりまや 橋 Kita Harimayaba bashi	はりまや橋 Harimaya bashi	蓮池町通 Hasuake machiuchi	高知橋 Kochi bashi	高知駅前 Kochi ekimae	JR高知駅 JR Kochi Station
2便	7:10		7:24	7:25	7:26	7:27	7:29	7:29	7:30	7:31	7:32
4便	7:35		7:52	7:53	7:54	7:55	7:57	7:57	7:58	7:59	8:00
6便	9:10		9:35	9:36	9:37	9:38	9:40	9:40	9:41	9:42	9:43
8便	9:15		9:40	9:41	9:42	9:43	9:45	9:45	9:46	9:47	9:48
10便	9:30		9:55	9:56	9:57	9:58	10:00	10:00	10:01	10:02	10:03
12便	9:35		10:00	10:01	10:02	10:03	10:05	10:05	10:06	10:07	10:08
14便	11:05		11:31	11:32	11:33	11:34	11:36	11:36	11:37	11:38	11:39
16便	11:10		11:36	11:37	11:38	11:39	11:41	11:41	11:42	11:43	11:44
18便	11:15		11:44	11:45	11:46	11:47	11:49	11:49	11:50	11:51	11:52
※1 ※2 20便	12:00		12:19	12:20	12:21	12:22	12:24	12:24	12:25	12:26	12:27
22便	12:40		12:59	13:00	13:01	13:02	13:04	13:04	13:05	13:06	13:07
24便	12:50		13:15	13:16	13:17	13:18	13:20	13:20	13:21	13:22	13:23
26便	13:40		13:59	14:00	14:01	14:02	14:04	14:04	14:05	14:06	14:07
28便	13:45		14:09	14:10	14:11	14:12	14:14	14:14	14:15	14:16	14:17
30便	14:05		14:30	14:31	14:32	14:33	14:35	14:35	14:36	14:37	14:38
32便	14:30		14:54	14:55	14:56	14:57	14:59	14:59	15:00	15:01	15:02
34便	15:10		15:37	15:38	15:39	15:40	15:42	15:42	15:43	15:44	15:45
36便	15:40		16:07	16:08	16:09	16:10	16:12	16:12	16:13	16:14	16:15
38便	15:50		16:16	16:17	16:18	16:19	16:21	16:21	16:22	16:23	16:24
40便	15:55		16:21	16:22	16:23	16:24	16:26	16:26	16:27	16:28	16:29
42便	17:45		18:16	18:17	18:18	18:19	18:21	18:21	18:22	18:23	18:24
44便	18:10		18:36	18:37	18:38	18:39	18:41	18:41	18:42	18:43	18:44
46便	18:30		18:56	18:57	18:58	18:59	19:01	19:01	19:02	19:03	19:04
48便	18:45		19:07	19:08	19:09	19:10	19:12	19:12	19:13	19:14	19:15
50便	20:00		20:22	20:23	20:24	20:25	20:27	20:27	20:28	20:29	20:30
52便	20:25		20:51	20:52	20:53	20:54	20:56	20:56	20:57	20:58	20:59
54便	20:30		20:52	20:53	20:54	20:55	20:57	20:57	20:58	20:59	21:00

到着便に合わせて運行致しますが、遅延により出発時刻が遅れる場合がございます。原則、航空機の到着予定時刻の5分後に設定している便が対応便となっております。

Airport to Kochi

Airport bus stop

One way: 740 yen



Program



1st WHEEL Seminar (5th IGS “Precambrian World 2023”)

March 5-6 Symposium in Kochi Core Center

March 5th

- 9:20** Welcome talk Sano Yuji
- 9:30** O-1 Secular Change of Atmospheric Oxygen Content through the Proterozoic and Crisis Evolution Hypothesis Tsuyoshi Komiya
The Univ. of Tokyo
- 10:00** O-2 In-situ Analysis of Carbonate-Associated Phosphate: Implications for Secular Change of Seawater Phosphate through the Precambrian Ryosuke Nagao
The Univ. of Tokyo
- Coffee break*
- 10:30** O-3 Micro-textural and Compositional Features in a Mesothermal Gold Mineralization at Akoase, Northeastern Axim-konongo (Ashanti) Belt, Ghana: Implications for Mining and Environmental Management Frank Nyame
Univ. of Ghana
- Relationship between Alteration and Mineralization in a Mesothermal Gold Prospect at Akoase, Northeastern Axim-konongo (Ashanti) Belt in the Birimian of Ghana
- 10:50** O-4 Stratigraphy and Age Relations in the Paleo-Proterozoic Birimian Rocks of the Cape Three Points Area, Southern Ashanti Greenstone Belt, Ghana Satoshi Yoshimura
Kyushu Univ.
- 11:20** O-5 Emergence of the Aerobic Atmosphere-Ocean System: Roles of Life and Earth’s Interior Andrey Bekker
Univ. of California
- 12:00** *Lunch*
- 13:20** O-6 Fluvial-Lacustrine Sediments Provenance Study of Malawi Stewart Ngalonde
Kyushu Univ.
- 13:40** O-7 Reconstructing of Antarctic Bottom Water Formation in the Cape Darnley over the Past 500,000 Years Keiko Takehara
Kochi Univ.
- 14:00** O-8 Enhanced Magmatism Triggered the Middle Miocene Climatic Optimum Kosuke T. Goto
Geological Survey of Japan, AIST
- Coffee break*
- 14:30** O-9 Nitrogen Bioavailability in the Late Paleoproterozoic Ocean Kento Motomura
Univ. of California
- 14:50** O-10 Silicate Spherules of Possible Impact Origin from the Paleoarchean Strelley Pool Formation, Western Australia Kenichiro Sugitani
Nagoya Univ.
- Coffee break*
- 15:30** O-11 The Belingwe Greenstone Belt, Zimbabwe – Some New Age Constraints and Implications for Greenstone Belt Evolution [Teams] Axel Hofmann
Univ. of Johannesburg
- 16:20** O-12 Remote Sensing and GIS for Monitoring Coastal Changes in El-Alamein Area, Matrouh, Egypt M.M. Abu El-Hassan
Menofia Univ.



1st WHEEL Seminar
(5th IGS “Precambrian World 2023”)

March 5-6 Symposium in Kochi Core Center

March 5th

Poster presentation

- 16:40** P-1 Are the Diamictites from the Eastern Desert of Egypt Represent Glacial Deposits??? The Regional and the Global Distribution and the Paleoclimatic Significance during the Pan-African Time
Mai El-Lithy
Menoufa Univ.
- P-2 Geochemistry and Tectonic Setting of Metavolcanic Rocks from the Cape Three Points Area in the Southern Ashanti Paleoproterozoic Birimian Greenstone Belt, Ghana
Kwabina Ibrahim
Univ. of Ghana
- P-3 Paleoenvironmental Changes off Antarctic Peninsula during Last 5,000 Years
Minoru Ikehara
Kochi Univ.
- P-4 A Review: Age Determination Methods of Marine Manganese Deposits
Takashi Ito
Ibaraki Univ.
- P-5 Occurrence and Geological Setting of a Neoproterozoic Ironstone in the Buem Structural Unit (BSU), Ghana
David Y. Ku
Ghana Geological Survey Authority
- P-6 Chaotic Beds in the Paleogene Muroto Formation at Muroto Peninsula, Kochi Prefecture, Japan
Hinako Matsumoto
Univ. of Kochi
- P-7 In Situ Sulfur Isotope Analysis of Sulfide in >3.95 Ga Metasedimentary Rocks: Sulfur Cycling and Microbial Activity in the Eoarchean
Ryota Mihori
The Univ. of Tokyo
- P-8 In-situ Analysis of Carbonate-associated Phosphate: Implications for Secular Change of Seawater Phosphate through the Precambrian
Takeshi Ohno
Gakushuin Univ.
- P-9 The Restoration of Sedimentary Environment of Mudstone Sequences in Goto Group, Nagasaki Prefecture, Japan
Hiroaki Takahashi
Kyushu Univ.
- P-10 Behavior of Phosphorous during the 2.7 Ga Submarine Hydrothermal Activities at Abitibi Greenstone Belt, Canada
Yuki Takashina
Univ. of Tohoku
- P-11 U-Pb Geochronology and Geochemistry in Zircon of the Utsubo Granitic Pluton, Hida Belt, Central Japan
Mami Takehara
National Institute of Polar Research
- P-12 Evidence for Early Ecosystem Preserved in Banded Iron Formation of the Isua Supracrustal Belt
Hikaru Tanabe
The Univ. of Tokyo
- P-13 Deformation Patterns of an Accretionary Prism Revealed by Sandbox Experiments
Satoshi Tonai
Kochi Univ.
- P-14 Reconstruction of Hydrothermal Oceanic Chert and Banded Iron Formation in Archean by Mineral Identification in Pilbara Terrane, Western Australia
Yusuke Inokuchi
Kyushu Univ.

17:10 *Poster session*

18:00 *Leave Core Center for party venue*

18:30 *Party at “Sea orchard” (海辺の果樹園)*



1st WHEEL Seminar
(5th IGS “Precambrian World 2023”)
March 5-6 Symposium in Kochi Core Center

March 6th

- | | | |
|--------------|---|--|
| 9:20 | O-13 Modern Iron Formation at Satsuma Iwo-jima Island, Kagoshima, Japan- Hydrothermal Chimney Mound, Iron Sediments and Iron Oolite. | Shoichi Kiyokawa
<i>Kyushu Univ.</i> |
| 9:50 | O-14 Paleoclimate And Paleoenvironmental Conditions during the Pan-african Orogeny in the Arabian-Nubian Shield: Implications From Iron Formations and Its Relation to Snowball Earth Hypnosis in the Eastern Desert, Egypt | Hanaa El Dokouny
<i>Univ. of Menoufia</i> |
| 10:10 | O-15 Re-Os Isotope Record in the Paleocene Limestone of the Chicxulub Impact Basin | Honami Sato
<i>Kyushu Univ.</i> |
| 10:30 | O-16 The Geology of Gold Mineralization in the Nangodi Greenstone Belt, Ghana | Fynn Kwame
<i>Univ. of Johannesburg</i> |
| | <i>Coffee break</i> | |
| 10:55 | O-17 Rare Earth Element Enrichment of the Late Ediacaran Kalyus Beds (Southwestern Baltica) through Diagenetic Uptake | Ion Francovschi
<i>Univ. of Bucharest</i> |
| 11:25 | O-18 Understanding Multistage Syntectonic Iron Ore Hypogene Mineralization in the São Francisco Craton – a Textural Approach | Alberto Carlos Rosière
<i>Universidade Federal de Minas Gerais (UFMG)</i> |
| 12:05 | <i>Lunch</i> | |
| 12:50 | <i>Core Center Tour</i> | |
| 13:40 | O-19 Phosphorous Cycle on the Archean Earth: Geological Constraints | Takeshi Kakegawa
<i>Univ. of Tohoku</i> |
| 14:20 | O-20 Paleontological and geochemical fingerprints of Iron-Oxidizing Bacteria from the ca. 1.88 Ga Gibraltar Granular Iron Formation | Alex Kovalick
<i>Univ. of California</i> |
| 14:50 | O-21 Hf-W Dating of Ancient Zircon Using a NanoSIMS | Yuji Sano
<i>Kochi Univ.</i> |
| 15:30 | O-22 Archaean Geology of the Singhbhum Craton, India: Insights from Greenstone Belts and Cratonic Cover Sequences
<i>[Teams]</i> | Jaganmoy Jodder
<i>Univ. of the Witwatersrand</i> |
| | <i>Coffee break</i> | |
| 16:00 | O-23 Trace Element and S-isotope Composition of Pyrite from the Witwatersrand Basin, South Africa | Andrea Agangi
<i>Akita Univ.</i> |
| 16:30 | O-24 Rapid Recovery of Strontium Isotope Compositions in the Ocean after the End-cretaceous Asteroid Impact (IODP Exp. 364 “Chicxulub Impact Crater”) | Kosei E. Yamaguchi
<i>Toho Univ.</i> |
| 17:00 | <i>Final talk</i> | Shoichi Kiyokawa
<i>Kyushu Univ.</i> |



Abstract



SECULAR CHANGE OF ATMOSPHERIC OXYGEN CONTENT THROUGH THE PROTEROZOIC AND CRISIS EVOLUTION HYPOTHESIS

Tsuyoshi Komiya¹

¹. Department of Earth Science and Astronomy, Graduate School of Arts and Sciences, The University of Tokyo, Tokyo 153-8902, Japan
komiya@ea.c.u-tokyo.ac.jp

1. Introduction

The origin and evolution of eukaryotes are key issues of biological evolution on the earth. It is widely considered that the eukaryotes first appeared after the Huronian Snowball Earth event and subsequent Great Oxidation Event (GOE), and multicellular eukaryotes, namely algae, emerged in the mid-Proterozoic. Because the eukaryotes need aerobic respiration, it was considered that atmospheric oxygen (pO₂) content was higher than the threshold of aerobic respiration, namely Pasteur point, through the Proterozoic (e.g. Kasting 1993; Lyons et al., 2014). Recently, the conventional view began to be reexamined (Lyons et al., 2021). For example, Cr isotopes of black shales suggest that the pO₂ contents remained lower than the threshold (Planavsky et al., 2018), and triple-oxygen isotopes of lacustrine sedimentary rocks may also support the low pO₂ condition (Planavsky et al. 2020; c.f. Liu et al., 2021). In addition, it is shown that even Metazoans can survive under low pO₂ condition (Mills & Canfield, 2014). On the other hand, high pO₂ condition in the Proterozoic was also proposed based on Iodine contents of carbonate minerals (e.g. Lu et al., 2018) and redox sensitive elements of pyrites (e.g. Large et al., 2019). We present a review of secular change of pO₂ contents and its influence on evolution of eukaryotes.

2. Results

The secular change of pO₂ content through the Proterozoic is enigmatic. We compiled redox sensitive element (RSE) contents of black shales, iodine contents of carbonate rocks and Cr isotopes of carbonate rocks to estimate pO₂ contents through the Proterozoic. RSE contents of pyrites may be also proxies for the pO₂ contents, but species of iron-bearing minerals are not used to estimate pO₂ contents because species of iron-minerals can discriminate anoxic/euxinic events from oxic periods but cannot differentiate oxic events/periods from anoxic/euxinic events/periods. Mercury (Hg) isotopes have a potential to quantitatively estimate pO₂ contents over 10⁻⁵ PAL in pO₂ contents. Previous studies showed that the pO₂ contents estimated from abundances of RSEs such as Mo increased gradually or stepwise through the Proterozoic (e.g. Scott et al., 2008), but their abundances were actually fluctuated. In fact, other proxies also show that the pO₂ contents were fluctuated through the Proterozoic, suggesting higher pO₂

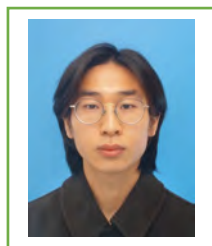
contents around 2.2, 1.5 and 0.8 Ga whereas lower around 1.7 and 1.0 Ga, respectively. On the other hand, molecular clock and paleontology suggest that appearance of eukaryotes, multicellular eukaryotes (algae), and Alveolata/Rhizaria around 2.1-1.9 Ga, 1.7, and 1.0 Ga, respectively (Strassert et al., 2021; Baludikay et al., 2016; Javaux & Lepot, 2018).

3. Discussion

Coevolution of organisms and the earth is widely discussed (e.g. Williams & Da Silva, 2003), and coevolution of eukaryotes and increase of pO₂ is often assumed in the Proterozoic (e.g. Condie & Sloan, 1998). However, the appearance of eukaryotes, namely symbiosis of aerobic bacteria within anaerobic archaea, occurred possibly in the high pO₂ period whereas other evolutions occurred possibly in the pO₂-poor periods. Because their precursors, namely anaerobic archaea and aerobic eukaryotes, need anoxic and oxic environments, respectively, it seems inconsistent between the evolutions and environments. We would like to propose that the contradiction is a driving force of evolution of eukaryotes, namely symbiosis, in the Proterozoic.

References

- Baludikay, B.K. et al., 2016. *Precambrian Research* **281**, 166-184.
- Condie, K.C., Sloan, R.E., 1998. *Origin and Evolution of Earth: Principles of Historical Geology*. Prentice Hall College Div, 498 pp.
- Javaux, E.J., Lepot, K., 2018. *Earth-Science Reviews* **176**, 68-86.
- Kasting, J.F., 1993. *Science* **259**, 920-926.
- Large, R.R., et al., 2019. *Mineralium Deposita* **54**, 485-506.
- Liu, P., et al., 2021. *Proceedings of the National Academy of Sciences* **118**, e2105074118.
- Lu, W., et al., 2018. *Science* **361**, 174-177.
- Lyons, T.W., et al., *Nature* **506**, 307-315.
- Lyons, T.W., et al., 2021. *Astrobiology* **21**, 906-923.
- Mills, D.B., Canfield, D.E., 2014. *BioEssays* **36**, 1145-1155.
- Planavsky, N.J., et al., 2018. *Emerging Topics in Life Sciences* **2**, 149-159.
- Planavsky, N.J., et al., 2020. *Astrobiology* **20**, 628-636.
- Scott, C., et al., 2008. *Nature* **452**, 456-459.
- Strassert, J.F.H., et al., 2021 *Nature Communications* **12**, 1879.
- Williams, R.J.P., Fraústo Da Silva, J.J.R., 2003. *Journal of Theoretical Biology* **220**, 323-343.



IN-SITU ANALYSIS OF CARBONATE-ASSOCIATED PHOSPHATE: IMPLICATIONS FOR SECULAR CHANGE OF SEAWATER PHOSPHATE THROUGH THE PRECAMBRIAN

Ryosuke Nagao^{1*}, Satoshi Yoshida², Yuki Ishihara¹, Yusuke Sawaki², Yuta Ijichi³, Takeshi Ohno⁴, Yuichiro Ueno⁵, Takafumi Hirata³, Tsuyoshi Komiya²

*corresponding author: ryo101112@g.ecc.u-tokyo.ac.jp

1. Department of Earth and Planetary Science, Graduate School of Science, The University of Tokyo, Bunkyo-ku, Japan
2. Department of Earth Science and Astronomy, Graduate School of Arts and Sciences, The University of Tokyo, Tokyo 153-8902, Japan
3. Geochemical Research Center, The University of Tokyo, Tokyo 113-0033, Japan
4. Department of Chemistry, Faculty of Science, Gakushuin University, Mejiro 1-5-1, Toshima-ku, Tokyo, 171-8588, Japan
5. Department of Earth and Planetary Sciences, Tokyo Institute of Technology, 2-12-1 Ookayama, Meguro-ku, Tokyo 152-8551, Japan

1. Introduction

Phosphorus is one of the most crucial bio-essential and bio-limiting elements and has a significant influence on the redox state of the earth's biosphere. It has been widely accepted that oxygenic photosynthesis may have emerged at least before the great oxidation event (GOE), but it is also considered that the Precambrian biosphere remained anoxic. This led to the proposal that the Precambrian primary productivity was severely limited by the low dissolved inorganic phosphate (DIP) levels through the Precambrian [1].

Shimura et al. 2014 [2] first proposed that the P contents in carbonate minerals can be used as a paleo-DIP proxy and showed that the seawater was enriched in Phosphate after the Marinoan glaciation. Recent works also validate that the P contents of carbonate minerals (termed carbonate-associated phosphate, or CAP), are a useful proxy [3-4]. Ingalls et al. 2022 [4] conducted whole-rock analysis by acid digestion for CAP in Neoproterozoic, but the data are highly scattered possibly due to the influence of minor clastic contamination and recrystallization. To avoid the effect of contaminations, we conducted an *in-situ* analysis of the carbonates using fs LA-ICP-MS at the Geochemical Research Center, the University of Tokyo, Japan. In this study, we present measured CAP/(Ca+Mg) ratios from late Archean to Phanerozoic shallow marine stromatolitic carbonates.

2. Results

Measured P/(Ca+Mg) ratios range from 0.03 to 1.10 mmol/mol in Neoproterozoic Tumbiana Formation, Western Australia; from 0.05 to 0.16 mmol/mol in Paleoproterozoic Duck Creek Formation, Western Australia; from 0.01 to 0.59 mmol/mol in Midproterozoic Khoraidi Formation, Nepal.


3. Discussion

We checked the time profiles of signal intensities of ICP-MS to detect the sign of contamination and exclude these data for a CAP comparison.

Secular change of CAP/(Ca+Mg) ratios shows that the Precambrian CAP contents tend to be larger than the contemporary counterpart. High to moderate CAP contents in Precambrian carbonates suggests that the DIP in the Precambrian Ocean was not scarce as previously suggested [1]. The apparent contradiction between the early emergence of oxygenic photosynthesis and the delayed rise of atmospheric P₀₂ should be reconciled by other explanations.

References

- [1] L. A. Derry, "Causes and consequences of mid-Proterozoic anoxia," *Geophys Res Lett*, vol. 42, no. 20, pp. 8538–8546, 2015, doi: <https://doi.org/10.1002/2015GL065333>.
- [2] T. Shimura et al., "In-situ analyses of phosphorus contents of carbonate minerals: Reconstruction of phosphorus contents of seawater from the Ediacaran to early Cambrian," *Gondwana Research*, vol. 25, no. 3, pp. 1090–1107, 2014, doi: [10.1016/j.gr.2013.08.001](https://doi.org/10.1016/j.gr.2013.08.001).
- [3] M. S. Dodd et al., "Development of carbonate-associated phosphate (CAP) as a proxy for reconstructing ancient ocean phosphate levels," *Geochim Cosmochim Acta*, vol. 301, pp. 48–69, May 2021, doi: [10.1016/j.gca.2021.02.038](https://doi.org/10.1016/j.gca.2021.02.038).
- [4] M. Ingalls, J. P. Grotzinger, T. Present, B. Rasmussen, and W. W. Fischer, "Carbonate-Associated Phosphate (CAP) Indicates Elevated Phosphate Availability in Neoproterozoic Shallow Marine Environments," *Geophys Res Lett*, vol. 49, no. 6, p. e2022GL098100, 2022, doi: <https://doi.org/10.1029/2022GL098100>.



Micro-textural and Compositional Features in a Mesothermal Gold Mineralization at Akoase, Northeastern Axim-Konongo (Ashanti) Belt, Ghana: Implications for Mining and Environmental Management

Frank K. Nyame*¹, Marian S. Sapah¹, Ibrahim Kwabina¹

1. Department of Earth Science, University of Ghana, Legon, Accra, Ghana

*Corresponding Author: fnyame@ug.edu.gh; fknnyame@yahoo.co.uk

Ore microscopy and Scanning Electron Microscope (SEM) investigations of ore and host rock samples taken from a gold prospect at Akoase in the northeastern part of the Axim-Konongo (Ashanti) belt has revealed intimate association of gold with pyrite (FeS_2) and, to a lesser extent, rare sphalerite (ZnS), generally contrasting with gold mineralization in many similar geological settings within the same belt where arsenopyrite (FeAsS) appears to be the dominant sulphide often associated with and/or used as pathfinder element in the search for gold mineralization. Gold in the Akoase mineralization identifiably occurs in fractures, as inclusions and/or occlusions in pyrite. It is possible that sub-microscopic gold grains occur in or associated with matrix quartz, carbonate and subordinate mica that are almost always present in the ore zone rocks. In general, rarity or absence of arsenopyrite (FeAsS) and galena (PbS) in many samples of both ore and host rocks investigated that could potentially contribute deleterious elements (e.g. arsenic and lead) suggests that the Akoase mineralisation may be mined and/or processed without much introduction of these potentially harmful elements into the surrounding environmental compartments.



Relationship between Alteration and Mineralization in a Mesothermal Gold Prospect at Akoase, Northeastern Axim-Konongo (Ashanti) Belt in the Birimian of Ghana

Frank K. Nyame*¹, Marian S. Sapah¹, Ibrahim Kwabina¹

1. Department of Earth Science, University of Ghana, Legon, Accra, Ghana

*Corresponding Author: fnyame@ug.edu.gh; fknyame@yahoo.co.uk

The gold prospect at Akoase in the northeastern flank of the Axim-Konongo (Ashanti) metavolcanic belt in the Birimian of Ghana appears to show distinct relationship between the nature of alteration of the gold bearing rocks and gold mineralization (as per the grade of gold). At the prospect scale, three main types of alteration patterns are present. The first, typified by the minerals chlorite, calcite and minor sericite, is the most dominant but rarely contains Au grades in excess of 0.5 g/t Au. The second most abundant alteration is represented by sericite, dolomite and minor chlorite and is associated with assays >1 g/t but less than 2 g/t Au. The third is usually characterized by sericite, ankerite and pyrite and samples show highly variable but comparatively high gold grades often in excess of 2 g/t Au. Considering that some prospects, separated by about 20-30 km, occur within narrow corridors of the generally northeast-trending shear system, identification of such alteration patterns in the rocks could greatly help narrow down on potentially mineralized zones during further exploration and/or deposit evaluation.



STRATIGRAPHY AND AGE RELATIONS IN THE PALEO-PROTEROZOIC BIRIMIAN ROCKS OF THE CAPE THREE POINTS AREA, SOUTHERN ASHANTI GREENSTONE BELT, GHANA

Satoshi Yoshimaru¹, Shoichi Kiyokawa¹, Takashi Ito², Kenji Horie³, Mami Takehara³, Kwabina Ibrahim⁴, George M. Tetteh⁵, and Frank K. Nyame⁴

1. Department of Earth and Planetary Sciences, Kyushu University, Fukuoka, Japan.
Yoshimaru.satoshi.536@s.kyushu-u.ac.jp
2. Ibaraki University, Mito, Japan.
3. National Institute of Polar Research, Tokyo, Japan.
4. University of Ghana, Legon, Ghana.
5. University of Mines and Technology, Tarkwa, Ghana.

1. Introduction

The Paleoproterozoic Birimian Supergroup covers a significant portion of the Leo-Man Shield of West Africa. The Birimian rocks have attracted numerous studies due, in part, to their importance as a host of significant gold and manganese mineralization and as a record of the Paleoproterozoic earth's evolution including known geological events such as the Great Oxidation Event and succeeding whole earth glaciation. The Birimian terrain is described as consisting of metasedimentary (mainly phyllite, greywacke, and subordinate volcanic) and meta-volcanic (basalt, andesite and minor phyllite and greywacke) rocks. These rocks are intimately associated with intrusives (Attoh, 1982). To date, there is not much agreement among various workers on aspects of Birimian geology such as the structure, stratigraphy, and age of Birimian rocks. This study was initiated in the Cape Three Points area at the southern Ashanti (Axim-Konongo) greenstone belt, Ghana. Because the area displays excellent exposures of fresh rocks along the coast, it is hoped that the outcome of the study could contribute greatly towards existing knowledge on Birimian geology especially the stratigraphy and formation age(s) of the rocks.

2. Geological Setting

The geology of the coastal Ashanti belt in Ghana has been described by various workers (e.g., Leube et al. 1990; Loh et al., 1999; Attoh et al., 2006). According to Loh et al. (1999), the Cape Three Points area is dominated by metavolcanic-volcaniclastic rocks (derived from Paleoproterozoic oceanic island arc volcano) associated with orogenic granitoid intrusions and an orogen-derived sedimentary cover unit (Tarkwaian rocks). It has been shown that the Birimian volcanic units are restricted to 2.17 Ga by the U-Pb zircon age of the Dixcove pluton.

Due to intense tropical weathering and forested vegetation, outcrops are generally scarce. However, the coastal Cape Three Points area presents very good exposures or outcrops. Loh et al. (1999) reported that the Birimian of the southern Ashanti belt is made up of three branches of which the intermediate is the Cape Three Points branch presented in this report.

3. Field Relations

The Cape Three Points branch has a 15 km long coastline with good rock exposures (Fig.1). In the field, this 15 km stretch could be further subdivided into west (lower), and east (upper) sections. Due to the lack

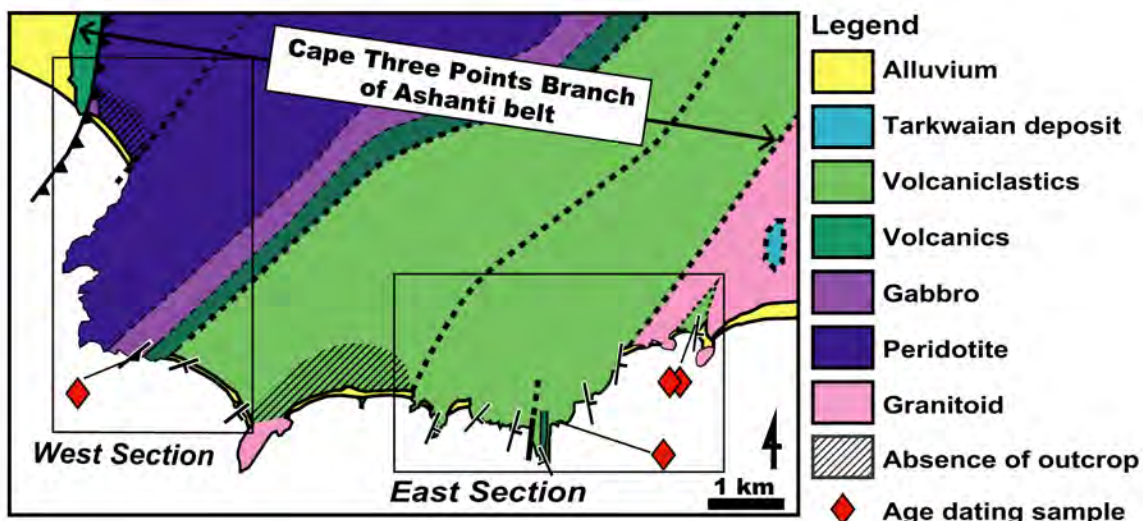


Fig. 1 Simplified geological map of the Cape Three Points branch of Ashanti belt.

of outcrops, a big stratigraphic gap separates the west (lower) from the east (upper) section and does not enable a complete reconstruction of the stratigraphy to be made. However, the field relationships of the rocks suggest they could form part or almost whole constituents of an ophiolite (or ophiolitic) sequence.

In the west section, an intensely brecciated crush zone marks a thrust fault that apparently obducts a magmatic-volcanic assemblage. It is composed of serpentized peridotite (dunite and harzburgite), foliated thin gabbro, lenticular or layered leucogabbro, hypabyssal and volcanic basalt with volcanoclastics. The east section exposes one thick volcanoclastic sequence up to 1500 m. The volcanoclastics are composed of turbiditic sandstone-mudstone alternations, breccia-bearing thick sandstone, and argillitic volcanic ash layers with minor components of meter-scale thick massive sandstone and accretionary lapilli layers/pods. The depositional features of the volcanoclastics strongly suggest distal facies of an island arc volcanic apron.

4. Age Relations

U-Pb zircon age dating of leucogabbro from the west section gave 2282 ± 0.57 Ma ($n=3$, MSWD=0.097, CA-ID-TIMS at Univ. of Toronto). This age indicates the timing of crystallization forming the gabbro from magma, thus implying the timing of the island arc basement (crust) development.

Quartz-Hornblende porphyry of the east section gave 2265.6 ± 4.6 Ma ($n=48$, MSWD=0.95, SHRIMP at National Institute of Polar Research: NIPR). Because this rock is cross-cutting the surrounding volcanoclastic metasedimentary rocks, the age indicates the minimum depositional age of those sedimentary rocks.

Two andesitic volcanoclastic sandstones occurring on the eastmost flank of the study area gave 2172.0 ± 6.1 Ma ($n=40$, MSWD=1.05, SHRIMP: NIPR) and 2172.6 ± 8.8 Ma ($n=35$, MSWD=1.07, SHRIMP: NIPR). Because the zircons are in sedimentary rock, the ages constrain their maximum depositional age.

5. Discussion

Based on the field relations so far, a working hypothesis can be proposed that the magmatic and clastic rock assemblage of the west and east sections formed one thick thrust sheet which together records tectono-magmatic activities and sedimentary process. The geochronological data suggested that the ages of the Birimian rocks are constrained c.a. 2.28-2.17 Ga. The depositional time range is constrained as 2.26-2.17 Ga for the volcanoclastic rocks of the east section. New age constraints revealed that the Birimian rocks of the study area were formed during the Paleoproterozoic environmental changes, which were likely synchronous with the Great Oxidation Event and glacial events.

References

- Attoh, K. (1982) Structure, gravity models and stratigraphy of a Paleoproterozoic volcanic sedimentary belt in northeastern Ghana. *Precambrian Research* **18**, 275-290
- Attoh et al. (2006) Geochemistry of an ultramafic-rodingite rock association in the Paleoproterozoic Dixcove greenstone belt, southwestern Ghana. *Journal of African Earth Sciences* **45**, 333-346
- Hirdes et al. (1992) Reassessment of Proterozoic granitoid ages in Ghana on the basis of U/Pb zircon and monazite dating. *Precambrian Research* **56**, 89-96.
- Leube et al. (1990) The Paleoproterozoic Birimian supergroup and some aspects of its associated gold mineralization. *Precambrian Research* **46**, 139-165
- Loh, G. et al. (1999) Explanatory Notes for the Geological Map of Southwest Ghana 1:100,000 Sekondi (0402A) and Axim (0403B) Sheets. *Hannover*



EMERGENCE OF THE AEROBIC ATMOSPHERE-OCEAN SYSTEM: ROLES OF LIFE AND EARTH'S INTERIOR

Andrey Bekker¹

1. Department of Earth & Planetary Sciences, University of California, Riverside;
andreyb@ucr.edu

1. Introduction

The Great Oxidation Event (GOE) refers to the transition from the mildly reducing Archean atmosphere-ocean system to the oxygenated atmosphere and shallow oceans of the early Paleoproterozoic that started at ~2.4 Ga and ended between 2.1 and 2.0 Ga (Holland 2002). The beginning and the end of the GOE were never explicitly defined. In general terms, the beginning of the GOE is marked by the disappearance of mass-independent fractionation of S isotopes and an increased range of mass-dependent fractionation of sulfur isotopes in association with highly variable carbon isotope record, Huronian glaciations, and the final stage in the assembly of the supercraton Superia (Bekker et al. 2004; Holland 2006; Bekker and Holland 2012; Gumsley et al. 2017). Although the term implies a relatively short duration, as that of phenomena used in event stratigraphy, the GOE is originally defined to last more than 200 Ma and finish at the end of the >2.22–2.06 Ga Lomagundi carbon isotope excursion during which between ~12 and 22 times the oxygen content of the present-day atmosphere was released to surface environments (Karhu and Holland 1996). While the internal texture of the GOE is still unresolved and remains to be a topic of further work (see Poulton et al. 2021), during these 200 Ma, atmospheric oxygen likely fluctuated across the level of 10⁻⁵ PAL (present atmospheric level) to a magnitude of fully oxygenated atmosphere (well below the modern level) before rapidly falling to much lower atmospheric and ocean oxygen concentrations in the immediate aftermath of the Lomagundi carbon isotope excursion (Ossa Ossa et al. 2018). The GOE ended up with the ocean deoxygenation in association with the supercraton Superia breakup, sea-level rise, and deposition of Mn- and P-rich sediments (Bekker et al. 2003).

2. Discussion

While the timing and texture of the GOE is progressively better understood (e.g., Gumsley et al., 2017; Warke et al. 2020; Poulton et al. 2021), mechanisms for delayed oxygenation remain highly speculative. The proposed diverse mechanisms can be broadly grouped into three categories relying on (1) changes in mantle properties, (2) continental crustal growth, and (3) progressive oxidation of continental or oceanic crust. Inferred changes in mantle properties, bearing on the surface redox

state, include oxidation of the mantle by crustal subduction and mantle overturn (Kump et al. 2000; Holland 2002) and progressive cooling of the upper mantle (Konhauser et al. 2009). Continental crustal growth is hold responsible for sea-level fall (emergence of landmasses; Bindeman et al. 2018) and increased subaerial volcanism during the Archean to Paleoproterozoic transition (Kump and Barley 2007; Gaillard et al. 2011), which resulted in delivery of more oxidized volcanic gases with respect to predominantly submarine volcanism in the Archean. Progressive oxidation of oceanic or continental crust by either hydrogen escape from the atmosphere or oxygenic photosynthesis is inferred in a number of models to either decrease oxygen sinks in the surface environments or increase oxidation potential of volcanic gases generated via crustal subduction and recycling (Holland 2009; Claire et al. 2006; Catling et al. 2001; Kasting 2013; Zahnle et al. 2013). All these models are concerned with the changes in the size of oxygen sinks and assume that the oxygen source did not change in size since oxygenic photosynthesis evolved.

An alternative could be that oxygenic photosynthesis was limited by low continental flux of nutrients (e.g., Mo and V; important for nitrogen fixation) into the Archean ocean or high removal potential of phosphorous in ferruginous ocean with green rust, iron oxyhydroxides, iron phosphates (Stüeken et al. 2021), resulting in limited net primary productivity and organic carbon burial. This suggestion is generally dismissed since it would have significant repercussions for the biogeochemical carbon cycle, which are not apparent in the carbon isotope record of Archean carbonates (e.g., Kasting 2013). However, continental weathering of sedimentary rocks would not return buried organic carbon to biogeochemical cycling under the Archean anoxic atmosphere; rather it would be buried again as recycled organic matter with sediments. Similarly, carbon isotope mass balance requires that carbon released by dissolution of sedimentary carbonates was also excluded from biogeochemical carbon cycle to satisfy carbon isotope values of Archean carbonates that are about 0‰. Consequently, carbon isotope records could be reconciled with limited net primary productivity and organic-carbon burial under the Archean anoxic atmosphere-ocean conditions.



Fluvial-Lacustrine Sediments Provenance study of Malawi

Stewart Ngalonde

Kyushu University (D2)

stewartngalonde@gmail.com

The Geology of Malawi was first mapped in 1960 by the British Geological Survey (BGS) at a scale of 100k and 250k. The revision of the Geology of Malawi, so as to update the maps and mineral occurrence knowledge, is a task that is still going. This work of remapping the Geology of Malawi began with the acquisition of Airborne Geophysical Survey Data (Magnetics, Radiometric and selected Gravity sites) in 2014. The ground work, as a follow-up to the airborne data, was started by the French Geological Survey (BRGM) in 2016 under the Geological Mapping and Mineral Assessment Project (GEMMAP). However, over 80% of the GEMMAP deliverables is more based on deskwork airborne Geophysical Survey data than ground work.

This current study, therefore, is aimed at complementing and filling gaps, as much as possible, so that we have a comprehensive and updated knowledge of the Geology and Mineral Occurrence of Malawi. The current study focusses on generating Fluvial-Lacustrine sand sediments, for detailed analysis, with a target of coming up with a provenance record of the Geology and Mineral occurrence of Malawi.

The Geology of North Malawi (the current target area) is controlled by Regional deformation histories largely controlled by the Ubendian-Usagaran belt, South of the Tanzania Craton. The Shear Zone, thus created from the belt, (Mughesse Shear Zone) traverses the extreme

Northern portion of North Malawi Geology, trending NW-SE, thereby dividing the North Malawi Geology into two Domains namely; the Ubendian and South Ubendian. These two Geological Domains represent the oldest Basement Rocks in the whole Malawi, at 2.1 to 1.8 Billion Years (Paleo to Meso Proterozoic).

At Local scale, the North Malawi Geology is affected by Rifting events belonging to the Karroo, at 230 Million Years (Permian to Triassic), and later by Miocene tectonics, at 8 Million Years (Dip-slip rift faults) attributed to the Malawi East African Rift System (EARS). The dominant river direction is Eastwards into Lake Malawi and therefore the Nyika Plateau (rising at 2,300m ASL) is the dominant topographic feature that define most river catchment in the area.

In the current fluvial and fluvial-lacustrine study, 43 sediment samples were collected, representing the major rivers and their catchment, as well as deltaic mouths on the lacustrine shores of Lake Malawi. The samples underwent Petrographic examination to identify dominant minerals and their spatial trends. The work is still ongoing, but current results agree with the Mafic terrane of the target area, the Biotite gneiss type rocks as well as Magnetic anomaly source areas for most magnetite grains.



Reconstructing of Antarctic Bottom Water formation in the Cape Darnley over the past 500,000 years

Keiko Takehara¹, Yuji Kato², Takuya Itaki³, Xiangyu Zhao⁴, Yusuke Suganuma⁵, Minoru Ikehara⁶

1. Graduate School of Integrated Arts and Sciences, Kochi University, Kochi, Japan
b20d6a01@s.kochi-u.ac.jp

- | | |
|---|--|
| <p>2. University of Tsukuba, Ibaraki, Japan
kato.yuji.ge@u.tsukuba.ac.jp</p> <p>3. Geological Survey of Japan, AIST, Ibaraki, Japan
t-itaki@aist.go.jp</p> <p>4. Shanghai Jiao Tong University, Shanghai, China
xy.zhao@sjtu.edu.cn</p> | <p>5. National Institute of Polar Research, Tokyo, Japan
suganuma.yusuke@nipr.ac.jp</p> <p>6. Center for Advanced Marine Core Research,
Kochi University, Kochi, Japan
ikehara@kochi-u.ac.jp</p> |
|---|--|

1. Introduction

Antarctic Bottom Water (AABW) is a vast heat and CO₂ reservoir that is closely linked to global climate change (Sigman and Boyle, 2000). However, the behavior of AABW formation during past interglacials remains unknown, making it difficult to predict its variability in response to future warming. Super-interglacial periods (MIS 5 and MIS 11) were about 1°C to 2°C warmer than the climate before the industrial revolution, making them ideal analogs for a warming Earth. This study aims to reconstruct the variability of Cape Darnley Bottom Water (CDBW) during the super-interglacial periods and to clarify which environmental factors may have caused changes in CDBW formation.

2. Results

WIC-6PC core (core length 12.7 m, water depth of 3153 m) was collected by R/V Hakuho-maru KH-20-1 cruise in Wild Canyon off Cape Darnley, East Antarctica. The top 5.8 m covers the pre-Holocene to MIS 11/12 boundary. For paleoenvironmental proxy, grain size composition, inorganic chemical composition, clay and heavy mineral composition, and diatom assemblages were used. This study used end-member modeling analysis (R-package EMMAgeo) to identify and quantify the depositional processes in sediments with multimodal grain size distribution. The end-members (EMs) are classified into four categories, with EM1 representing suspended load and EM4 representing iceberg rafted debris (IRD). On the other hand, EM2 represented silt particles affected by near-bottom water advection, while EM3 reflected stronger flow. The heavy minerals in WIC-6PC are mainly composed of almandine garnet, and the redox index Mn/Fe is high before the peaks of EM3 and EM2, indicating the oxidation state of the seafloor.

3. Discussion

Since almandine garnet is a heavy mineral characteristic of the Cape Darnley area (Borchers et al., 2011) and AABW is oxidative (Murakami et al., 2020), EM2 and EM3 show the CDBW advection under

different flow velocities. Changes in the EMs indicate that strong CDBW flow occurred during the interglacial period from MIS 5 to MIS 9. However, MIS 11 showed weakened CDBW formation.

Possible factors for the decrease in CDBW formation are fresh water supply from melting ice sheets and sea ice. Sea ice-related diatoms and *Chaetoceros* resting spores showed a decreased abundance during MIS 11. In the Southern Ocean, *Chaetoceros* resting spore has been associated with the presence of sea ice meltwater (Abelmann et al., 2006). Therefore, these data suggest that the Wild Canyon area was a less sea-ice environmental setting during MIS11. In addition, there were no significant peaks in IRD and chrysophyte cyst (freshwater algae), which are indicators of ice sheet melting.

From the above, it is concluded that the weak CDBW flow during MIS 11 is due to the reduced influence of sea ice. Previously, melting ice was thought to be the primary cause of the decline in AABW formation, but our data suggest that sea ice loss may also be a significant contributor.

References

- Abelmann, A., Gersonde, R., Cortese, G., Kuhn, G. and Smetacek, V. (2006) Extensive phytoplankton blooms in the Atlantic sector of the glacial Southern Ocean. *Paleoceanography* **21**, PA1013.
- Borchers, A., Voigt, I., Kuhn, G. and Diekmann, B. (2011) Mineralogy of glaciomarine sediments from the Prydz Bay–Kerguelen region: relation to modern depositional environments. *Antarctic Science* **23**, 2, 164-179.
- Murakami, K., Nomura, D., Hashida, G., Nakaoka, S., Kitade, Y., Hirano, D., Hirawake, T., Ohshima, K. I. (2020) Strong biological carbon uptake and carbonate chemistry associated with dense shelf water outflows in the Cape Darnley polynya, East Antarctica. *Marine Chemistry* **225**, 103842.
- Sigman, D.M., and Boyle, E.A. (2000) Glacial/interglacial variations in atmospheric carbon dioxide. *Nature* **407**, 6806, 859-869.



ENHANCED MAGMATISM TRIGGERED THE MIDDLE MIOCENE CLIMATIC OPTIMUM

Kosuke T. Goto¹

1. Geological Survey of Japan, AIST, Tsukuba, Japan

1. Introduction

The middle Miocene Climatic Optimum (MCO) represents one of the most prominent warming events during the Cenozoic, and was accompanied by a long-lasting positive $\delta^{13}\text{C}$ excursion e.g., (Steinthorsdottir et al., 2021) The MCO was likely tied to accumulation of atmospheric CO_2 , and may have affected the evolution of terrestrial organisms. However, little is known about the underlying processes responsible for the perturbations in the Miocene climate and global carbon cycle. Here, we report high resolution middle Miocene seawater Os isotope data derived from marine sediments from Ocean Drilling Program (ODP)/ International Ocean Discovery Program (IODP) cores and the results of numerical modeling of the global carbon cycle.

2. Results

Our data reveal a negative Os isotope excursion from 0.80 to 0.72, with the lowest values at ~ 17 – 15.8 Ma. The observed Os isotope anomaly can be explained by a ~ 22 – 45% increase in non-radiogenic Os input from the mantle into the ocean. The carbon cycle model demonstrates that such an increase in magmatism is capable of elevating atmospheric $p\text{CO}_2$ by 65–1440 ppmv and of causing a positive excursion in seawater $\delta^{13}\text{C}$ of 0.4–0.8‰, which is generally consistent with geological and geochemical observations.

3. Discussion

It is conceivable that enhanced magmatism, such as the eruption of the Columbia River flood basalts, rapid seafloor spreading, and/or a pulse of arc volcanism, triggered the fluctuations in climate and the global carbon cycle during the middle Miocene (e.g., Dalton et al., 2022; Kasbohm et al., 2018). Evidence for enhanced magmatism during the middle Miocene also helps explain the contemporaneous diversification of browsing ungulates in C3-dominated ecosystems (Janis et al., 2000).

References

- Dalton, C. A., Wilson, D. S. & Herbert, T. D. Evidence for a global slowdown in seafloor spreading since 15 Ma. *Geophys. Res. Lett.* **49**, e2022GL097937 (2022).
- Janis, C. M., Damuth, J. & Theodor, J. M. Miocene ungulates and terrestrial primary productivity: where

have all the browsers gone? *Proc. Natl. Acad. Sci. USA* **97**, 7899–7904 (2000).

Kasbohm, J. & Schoene, B. Rapid eruption of the Columbia River flood basalt and correlation with the mid-Miocene climate optimum. *Sci. Adv.* **4**, eaat8223 (2018).

Steinthorsdottir, M., et al. The Miocene: the future of the past. *Paleoceanogr. Paleoclimatol.* **36**, e2020PA004037 (2021).



NITROGEN BIOAVAILABILITY IN THE LATE PALEOPROTEROZOIC OCEAN

Kento Motomura¹, Andrey Bekker¹, Minoru Ikehara², Wouter Bleeker³ and Shoichi Kiyokawa⁴

1. Department of Earth and Planetary Sciences, University of California, Riverside, California, USA

2. Center for Advanced Marine Core Research, Kochi University, Kochi, Japan

3. Geological Survey of Canada, Ottawa, Ontario, Canada

4. Department of Earth and Planetary Sciences, Kyushu University, Fukuoka, Japan

1. Introduction

The late Paleoproterozoic was a key period in evolution of Earth's surface environment and life. It is suggested that the ca. 2.4 Ga Great Oxidation Event raised atmospheric oxygen levels to an intermediate state and greatly changed chemical compositions of the ocean (Poulton et al., 2021; Bekker, 2022). Eukaryotes could have appeared during the late Paleoproterozoic, but divergence of complex animals has been suppressed until the Neoproterozoic (Javaux and Lepot, 2018). Low nitrate bio-availability during the Proterozoic potentially links to the delayed eukaryote evolution since nitrogen is an essential nutrient for life (Anbar, 2008; Stüeken et al., 2016). Here we examine bio-availability of nitrogen in the late Paleoproterozoic ocean, with determination of nitrogen isotope compositions of black shales preserved in the ca. 1.9 Ga Nuvilik Formation of the Povungnituk Group, Cape Smith belt, Canada.

2. Results and Discussion

Two diamond drill-holes (DDHs) 718-3333 (~50-m-long) and 4G8069 (~80-m-long) investigated in this study consist of turbiditic greywacke–black shale alternations deposited on the continental margin of the Archean Superior craton (below storm wave base). Lithostratigraphically, turbiditic deposits in DDH 4G8069 are relatively predominated by sandstones than those in DDH 718-3333. Depositional environments are inferred as above and near redoxcline for DDHs 4G8069 and 718-3333, respectively. Nitrogen isotope compositions suggest elevated values ($> +1\%$) in all the black shale samples, representing aerobic nitrogen cycling and existence of bio-available nitrate on the Superior margin. Moreover, nitrogen isotope values of DDH 718-3333 are ~2‰ higher than those of DDH 4G8069. The isotopic heterogeneity is similar to that observed in modern oxygen minimum zones (Mollier-Vogel et al., 2012) and could represent enhanced denitrification in sulfidic water column. Although no unambiguous microfossils of ca. 1.9 Ga eukaryote have been reported, the aerobic nitrogen cycling observed in the Nuvilik Formation is consistent with molecular clock studies suggesting emergence of eukaryotes during the late Paleoproterozoic (Betts et al., 2018). However, offshore nitrate reservoir could have contracted at the end of the Paleoproterozoic, as

suggested by lowered nitrogen isotopic compositions in the Mesoproterozoic offshore deposits (Koehler et al., 2017). Additional nitrogen and microfossil studies will elucidate the timing of eukaryote evolution and its implications for nitrogen cycling.

References

- Anbar, A.D. (2008) Oceans. Elements and evolution. *Science* **322**, 1481–1483.
- Bekker, A. (2022) Great Oxidation Event. In: Gargaud, M., Irvine, W.M., Amils, R., Claeys, P., Cleaves, H.J., Gerin, M., Rouan, D., Spohn, T., Tirard, S., Viso, M. (Eds.), *Encyclopedia of astrobiology*. Springer, Berlin, Heidelberg, pp. 1–9.
- Betts, H.C., Puttick, M.N., Clark, J.W., Williams, T.A., Donoghue, P.C.J. and Pisani, D. (2018) Integrated genomic and fossil evidence illuminates life's early evolution and eukaryote origin. *Nat. Ecol. Evol.* **2**, 1556–1562.
- Javaux, E.J. and Lepot, K. (2018) The Paleoproterozoic fossil record: Implications for the evolution of the biosphere during Earth's middle-age. *Earth-Sci. Rev.* **176**, 68–86.
- Koehler, M.C., Stüeken, E.E., Kipp, M.A., Buick, R. and Knoll, A.H. (2017) Spatial and temporal trends in Precambrian nitrogen cycling: A Mesoproterozoic offshore nitrate minimum. *Geochim. Cosmochim. Acta* **198**, 315–337.
- Mollier-Vogel, E., Ryabenko, E., Martinez, P., Wallace, D., Altabet, M.A. and Schneider, R. (2012) Nitrogen isotope gradients off Peru and Ecuador related to upwelling, productivity, nutrient uptake and oxygen deficiency. *Deep-Sea Res. Part 1, Oceanograph. Res. Pap.* **70**, 14–25.
- Poulton, S.W., Bekker, A., Cumming, V.M., Zerkle, A.L., Canfield, D.E. and Johnston, D.T. (2021) A 200-million-year delay in permanent atmospheric oxygenation. *Nature* **592**, 232–236.
- Stüeken, E.E., Kipp, M.A., Koehler, M.C. and Buick, R. (2016) The evolution of Earth's biogeochemical nitrogen cycle. *Earth-Sci. Rev.* **160**, 220–239.



SILICATE SPHERULES OF POSSIBLE IMPACT ORIGIN FROM THE PALEOARCHEAN STRELLEY POOL FORMATION, WESTERN AUSTRALIA

Kenichiro Sugitani¹, Koichi Mimura¹, Ryoko Senda², Yui Kouketsu¹, Simon Wallis³, Natsuko Takagi⁴, Tsuyoshi Iizuka³, and Donald R. Lowe⁵

1. Department of Earth and Planetary Sciences, Nagoya University, Japan, sugi@info.human.nagoya-u.ac.jp
2. Graduate School of Social and Cultural Studies, Kyushu University, Japan
3. Department of Earth and Planetary Science, University of Tokyo, Japan
4. Technical Center, Nagoya University, Japan.
5. Department of Geological Sciences, Stanford University, USA.

1. Introduction

Large asteroid impacts are thought to have occurred frequently from the Archean to the Paleoproterozoic (e.g., Lowe and Byerly, 2018). This is based mainly on identification of "impact layers" containing silicate spherules formed by condensation of vaporized impactors and targets by bombardments. Such extraterrestrial impacts likely influenced the Earth's early environment, including crustal deformation, evaporation of significant volumes of ocean water, and might have even triggered the modern-style plate tectonics (Lowe, 2013). In this study we describe newly discovered silicate spherules of possible impact origin from the ca. 3.4 Ga Strelley Pool Formation (SPF) of the Pilbara Craton, Western Australia, from which widely accepted biosignatures, including stromatolites and microfossils of various shapes have been identified (Allwood et al., 2006; Sugitani et al., 2010). Spherules have been identified from the two localities in the Panorama and the Goldsworthy greenstone belts. Here the Panorama spherules are mainly described, and their origins are discussed.

2. Results

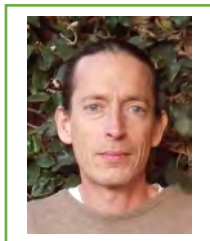
At the Panorama locality, spherules occur in a thin clastic later intercalated with microfossil-bearing black chert. The clastic layer is enriched in angular to subrounded sedimentary fragments (rip-up clasts). Spherules, which occur as individual framework grains and within clasts, have various morphologies (completely spherical to angular), sizes (20 μm to >500 μm), textures (layered, non-layered, and fibrous), mineralogy (various proportions of microcrystalline quartz, sericite, anatase and Fe-oxides), and chemistry (enriched in Ni and/or Cr), commonly with thin anatase-rich walls. Spherule-rich layers are enriched in platinum group elements and clastic-derived elements such as Al, Ti and Zr. Elemental mapping showed that the spherules, if not all, tended to be enriched in Cr and/or Ni. Spherules with buds and coalesced spherules were present, although the majority were single. Lath-shaped crystal relicts and stellate anatase crystals had rarely been identified.

3. Discussion

Origins other than asteroid impact for the SPF spherules, such as sedimentary, volcanic, and meteorite ablation were considered. However, any of them cannot reliably explain the SPF spherules. While the origins of many SPF spherules were poorly constrained, the most promising types as impact origin were non-layered spherical spherules. For the SPF spherule's case, platinum group elements could not provide any constraints on the origin of spherules. Therefore, other data, such as the isotopic composition of Cr, would be required to confirm the impact origin of the SPF spherules.

References

- Allwood, A.C., Walter, M.R., Kamber, B.S., Marshall, C.P., Burch, I.W. (2006) Stromatolite reef from the Early Archaean era of Australia. *Nature* **441**, 714-718.
- Lowe, D.R. (2013) Crustal fracturing and chert dike formation triggered by large meteorite impacts, ca. 3.260 Ga, Barberton greenstone belt, South Africa. *Geol. Soc. Am. Bull.* **125**, 894-912.
- Lowe, D.R. and Byerly, G.R. (2018) The terrestrial record of Late Heavy Bombardment. *New Astronomy Rev.* **81**, 39-61.
- Sugitani, K., Lepot, K., Nagaoka, T., Mimura, K., Van Kranendonk, M.J., Oehler, D.Z., Walter, M.R. (2010) Biogenicity of morphologically diverse carbonaceous microstructures from the ca. 3400 Ma Strelley Pool Formation, in the Pilbara Craton, Western Australia. *Astrobiology* **10**, 899-920.



THE BELINGWE GREENSTONE BELT, ZIMBABWE – SOME NEW AGE CONSTRAINTS AND IMPLICATIONS FOR GREENSTONE BELT EVOLUTION

Axel Hofmann¹, Xian-Hua Li², Dwight C. Bradley³, Fabien Humbert⁴

1. Department of Geology, University of Johannesburg, Johannesburg, South Africa.

ahofmann@uj.ac.za

2. Institute of Geology and Geophysics, Chinese Academy of Sciences, Beijing, China.

lixh@gig.ac.cn

3. Dartmouth College, Hanover, USA. bradleyorchard2@gmail.com

4. University of Rennes, Rennes, France. fabien.humbert@univ-rennes1.fr

The Neoarchaean Belingwe greenstone belt of the Zimbabwe craton consists of a well-preserved succession of rocks of very low metamorphic grade and low strain. We present new age constraints for the Ngezi Group of the belt and discuss them in the light of greenstone belt evolution. We propose crustal destabilization of the Zimbabwe proto-craton as a result of global convective mantle overturn at ~2.75 Ga. This gave rise to extension of a Mesoarchaeon granitoid-greenstone terrain, rapid subsidence and, initially, deposition of a transgressive cover succession (Manjeri Formation). High degrees of

stretching of proto-cratonic and mantle lithosphere provided accommodation space for the emplacement of several kilometres of submarine volcanic rocks on deeply submerged granitoid-greenstone basement, herein referred to as proto-cratonic flood basalts. Once extension and magmatism had ceased, chemical and clastic sedimentary rocks of the Cheshire Formation were deposited prior to 2.71 Ga as a result of, and subjected to, compressional deformation, and much earlier than previously assumed.



Remote sensing and GIS for monitoring coastal changes in El-Alamein area, Matrouh, Egypt

Hanaa A. Hammad¹, Ahmed M. El-Zeiny¹, M.M. Abu El-Hassan², Moataz M. Khalifa²

1. Environmental Studies Department, National Authority for Remote Sensing and Space Sciences (NARSS), Egypt

2. Geology Department, Faculty of Sciences, Menofia University
abouelhassanmohamed@gmail.com

Coastal areas are very dynamic because they are influenced by different anthropogenic and natural factors. Therefore, it is very important to assess the temporal changes in land use and land cover (LULC), and shoreline. The present study aims to monitor changes in shoreline and LULC in the El-Alamein area, Egypt. Radiometrically corrected multi-temporal Landsat images dated 2000, 2010, and 2020 were processed to produce LULC maps and to delineate shorelines to assess changes using ENVI 5.3 and ArcGIS 10.5. A field trip was conducted to identify the main LULC units and to improve the resultant maps. Results showed that the El-Alamein coastal area was greatly impacted by land reclamation and urban growth in the last two decades, with urban areas increasing from 11.13 km² in 2000 to 22.67 km² in 2010 to 55.83 km² in 2020. Further, the vegetation class increased from 15.63 km² in 2000 to 52.17 km² in 2010 to 86.41 km² in 2020. Shoreline

maps show that the total areas of accretion and erosion were 1.3380 and 0.3067 km² during (2000-2010), as well as 0.3541 and 0.6205 km² during (2010-2020), respectively. A higher rate of accretion was reported in the first period (2000–2010), while in the second period (2010–2020), erosion was predominant. It can be concluded that the El-Alamein coastal area is considered one of the pioneering regions of development that showed a positive impact on the land resources. It's recommended to regularly assess the changes that might occur to mitigate the potential hazard.

Keyword:

Remote sensing, shoreline changes, land use/cover, El-Alamein



Modern Iron formation at Satsuma Iwo-Jima Island, Kagoshima, Japan- Hydrothermal chimney mound, iron sediments and iron oolite.

Shoichi Kiyokawa^{1,2,3}

1. Department of Earth and Planetary Sciences, Kyushu University, Fukuoka, Japan.
2. Center for Advanced Marine Core Research, Kochi University
3. Department of Geology, University of Johannesburg
kiyokawa@geo.kyushu-u.ac.jp

1. Introduction

Ancient iron sediments have been used as key markers of oxidation events in Earth's history. The formation of many BIFs is thought to be associated with major increases in atmospheric oxygen concentration. However, microbiogenic oxidation systems may present more convincing models for the formation of iron sediments under anoxic conditions on the ocean floor (e.g. Bekker, 2010; Konhauser et al., 2017). Nagahama Bay at Satsuma Iwo-Jima Island, Japan, well preserved several 3 types iron formation were identified within a fishing port in this bay. thick piles of oxyhydroxide sediments accumulate at high sedimentation rates in an orange-colored turbid water mass (Kiyokawa and Ueshiba, 2015). Details of the microbial activity at this site have already been reported by Hoshino et al. (2016). However, the depositional environment in this bay area remains poorly understood. We carried out long-term observational studies of the water column in the fishing port though diving expeditions, camera monitoring, and by generating records of seawater conditions (pH, temperature, turbidity). Result of these works, we identified turbid water movement by tidal, wind and typhoon effects (Ninomiya and Kiyokawa, 2009). We identified a rare very clear (low turbidity) water condition in the fishing port as well as a thick iron-rich sedimentary sequences preserved at a site in the west of the fishing port. Oxyhydroxide mounds within a site in the east of the fishing port (Kiyokawa et al., 2020).

2. Results

- 1) **Iron mound:** The mounds are made of two types of material: hard, dark brown–orange, high-density material; and soft, brownish orange–yellow, low-density material. Computed tomography scans of the harder iron mound material revealed a cabbage-like structure consisting of micropipe structures with diameters of 2–5 mm. These micropipes have relatively hard walls made of iron oxyhydroxides (FeOH) and are identified as discharge pipes. Nucleic acid staining genetic sequencing and scanning electron microscope observations suggest that the mounds formed mainly from bacterial stalks with high concentrations of FeOH colloidal matter. In the harder parts of the mounds, these “fat stalks,” which contain oxyhydroxide colloidal aggregates, are entwined and concentrated. The softer material contains twisted stalk-like structures, which are coated with FeOH colloidal particles. Eoxryri bonucleic acid (DNA) examination of the iron mounds revealed the presence of iron-oxidizing bacteria, especially at the mound surface.
- 2) **Iron sediment:** At west side of the fishing port, thick FeOH sediments well preserved. 15 years continuous sediment traps and sediment core was collected in this site. Sedimentation rate at the west site was between 2.8 and 4.9 cm/yr (based on cores taken from the seafloor) and 33.3 cm/yr (based on sediment traps). 50-100m deep portion of sediment core identified the siderite crystal formed.
- 3) **Iron oolite:** Along the beach of the Nagahama bay, there are iron oolite identified. They covered by less than 10 μm

thick laminated FeOH matter. Some of scoop of sand grains, microbial texture.

3. Conclusion

There are areas in Nagahama Bay where iron mounds are forming within a dense, orange-colored, turbid sea via a combination of chemical and biological activity. There are also areas where FeOH sediments are accumulating through chemical precipitation alone, where oxidized colloidal matter grows at the sediment surface. Influence of FeOB biofilm activity at chimneys leads to much higher rates of FeOH sedimentation than when deposition only occurs via chemical sedimentation of colloids. Indeed, it is estimated that accumulation rates are ~9–15 times higher in the biogenically influenced iron mounds than in the iron colloidal sediments.

Furthermore, the iron mounds appear to be more resistant to erosion due to the presence of biogenic stalk-like structures. The role of biogenic activity in the formation of iron-rich sediments may have played a major role in the preservation of iron-rich silica associated with low-temperature hydrothermal sequences in the geological record. FeOB at shallow-marine hydrothermal vents may be analogous to the depositional environment of some ancient iron formations.

References

- Bekker, A., Slack, J., Planavsky, N., Krapež, B., Hofmann, A., Konhauser, K.O., and Rouxel, O.J., 2010, Iron formation: The sedimentary product of a complex interplay among mantle, tectonic, oceanic, and biospheric processes: *Economic Geology and the Bulletin of the Society of Economic Geologists*, v. 105, p. 467–508, <https://doi.org/10.2113/gsecongeo.105.3.467..>
- Hoshino, T., Kuratomi, T., Morono, Y., Hori, T., Oiwane, H., Kiyokawa, S., and Inagaki, F., 2016, Ecophysiology of Zetaproteobacteria associated with shallow hydrothermal iron-oxyhydroxide deposits in Nagahama Bay of Satsuma Iwo-Jima, Japan: *Frontiers in Microbiology*, v. 6, no. 1554, p. 1–11, <https://doi.org/10.3389/fmicb.2015.01554>.
- Konhauser, K.O., Planavsky, N.J., Hardisty, D.S., Robbins, L.J., Warchola, T.J., Haugaard, R., Lalonde, S.V., Partin, C.A., Oonk, P.B.H., Tsikos, H., Lyons, T.W., Bekker, A., and Johnson, C.M., 2017, Iron formations: A global record of Neoproterozoic to Palaeoproterozoic environmental history: *Earth-Science Reviews*, v. 172, p. 140–177, <https://doi.org/10.1016/j.earscirev.2017.06.012>.
- Kiyokawa S., Kuratomi T., Hoshino T., Goto S., Ikehara M., 2021, Hydrothermal formation of iron-oxyhydroxide chimney mounds in a shallow semi-enclosed bay at Satsuma Iwo-Jima Island, Kagoshima, Japan. *Geological Society of America Bulletin*, 133 (9-10): 1890–1908. <https://doi.org/10.1130/B35782.1>.
- Kiyokawa, S., and Ueshiba, T., 2015, Rapid sedimentation of iron oxyhydroxides in an active hydrothermal shallow semi-enclosed bay at Satsuma Iwo-Jima Island, Kagoshima, Japan: *Sedimentary Geology*, v. 319, p. 98–113, <https://doi.org/10.1016/j.sedgeo.2015.01.010>.
- Ninomiya, T., and Kiyokawa, S., 2009, Time-series measurement of colored volcanic vent seawaters during a tidal cycle in Nagahama Bay, Satsuma Iwo-Jima Island, Kagoshima, Japan: *Memoirs of the Faculty of Sciences, Kyushu University, Series D: Earth and Planetary Science*, v. 32, p. 1–14.



Paleoclimate and Paleoenvironmental Conditions during the Pan-African Orogeny in the Arabian-Nubian Shield: Implications from Iron Formations and its relation to Snowball Earth hypnosis in the Eastern Desert, Egypt

Hanaa El Dokouny¹

1. Department of Geology, University of Menoufia, Menoufia, Egypt
hanaaabdelnaby4@gmail.com

1. Introduction

Thirteen BIF occurrences are recorded in the central Eastern Desert (CED) of Egypt that represents the northwestern part of the Arabian–Nubian Shield and comprise Neoproterozoic basement rocks formed during the Pan Africa Orogeny.

2. Age, Geological setting and mineralogy

Various localities of BIF in CED bear high similarities in geological setting and mineralogy. They occur as rhythmically layered bands or separate lenses with thickness up to 100m intercalated with Neoproterozoic volcanic arc assemblages dominated by andesitic lava flows, tuffs and lapilli tuffs. Oxide (predominately magnetite) and silicate facies ubiquitous; carbonate facies (usually calcite) is common in several deposits. Sulfide facies is generally lacking. In most cases, the BIFs contain syn-sedimentary bedding and lamination. The entire sequence of BIFs and host rocks is regionally metamorphosed under greenschist to amphibolite facies conditions which later deformed during convergence produced secondary hydrothermal fluid resulting in development of second sulfide generation hosting gold.

3. Origin of Egyptian BIFs

There are two common genetic models of Egyptian BIFs: 1) precipitation following submarine volcanism in an island arc setting suggesting a linkage between the Egyptian BIF and the Algoma-type BIF (Abd El-Rahman et al., 2019); 2) precipitation after the melting of glacial ice during an interglacial period of the Snowball Earth hypnosis, which is consistent with the presence of diamictites intercalated with at least one of these BIF deposits comparable to the Rapitan type BIF (Stern et al., 2013). BIF has much lower contents of Al₂O₃, Na₂O, K₂O, Ni, Co, Cr, and Sr and higher amounts of MnO, TiO₂, P₂O₅, Cu, and Zn than the hosting tuffs. Moreover, BIF have negative Eu anomalies, depleted HREE, and NASC-normalized La/Nd ratios <1, either slightly negative or positive cerium anomalies. These features are dissimilar to hydrothermal-genetic Brokman iron formation (Derry&Jacobsen 1990) and speak against a volcanogenic origin for the BIFs. Source of Fe and Si were thought to be leached out from solidified volcanic rocks by heated sea and ground waters that were discharged to the basin. BIFs contain few amounts of TiO₂, Al₂O₃, Na₂O, and K₂O indicating the presence of few detritus where the island-arcs are envisaged as a

mature landscape, characterized by slow-running rivers transporting dissolved and very fine-grained particles, which were ultimately deposited in the shallow small basins.

4. Dissimilarity of Egyptian BIFs with Algoma- and Rapitan-types of BIFs

The Egyptian BIFs form unique lithostratigraphic units different from the known Algoma and Rapitan types of BIF. BIF shows slight elevated Fe, Ti, Mg, Ca, and P and depressed Si, Mn, Al, and K values compared to the Algoma type. However high Fe and P in Egyptian BIFs are akin to Rapitan-type BIFs as well as relative similarity of their REEs patterns (El Dokouny, 2017), glacial deposits capped by carbonate rocks associated to Rapitan BIF is missing in the Egyptian BIFs. So, another model may be proposed for BIF precipitation. Organic matter including the humble blue-green algae, blue-green bacteria, or cyanobacteria is recorded in El Dabbah and Wadi Kareim BIFs, CED (El Habaak 2001). Recent studies on El Dabbah BIF concluded that BIF formed biologically in anoxic environment (El Dokouny, 2017; Kiyokawa et al., 2020). This study believes in the role of biological role in BIF precipitation specially by primitive anoxygenic photosynthetic bacteria. Ferric hydroxide is directly precipitated through the oxidation of ferrous iron by this kind of bacteria. Besides, the study conclude that Sturtian glaciation recorded in other locations all over the world may be the reason of anoxic condition prevailing during BIF formation though presence of glacial deposits in CED is not clear and need more studies.

References

- Abd El-Rahman, Y., Gutzmer, J., Li, X., Seifert, T., Li, C., Ling X. & Li J., (2019). Not all Neoproterozoic iron formations are glaciogenic: Sturtian-aged non-Rapitan exhalative iron formations from the Arabian–Nubian Shield. *Mineralium Deposita*. <https://doi.org/10.1007/s00126-019-00898-0>
- Derry L.A., & Jacobsen, S.B., (1990). The chemical evolution of Precambrian seawater: evidence from REEs in banded iron formations. *Geochim Cosmochim Acta* 54:2965–2977.
- El-Dokouny, H.A., (2017). *Geochemical and Isotopic Studies of Some Neoproterozoic Banded Iron Formations from the Eastern Desert of Egypt: Insights into ‘Snowball Earth’ Seafloor*

- Environments. Unpublished PhD Thesis, Menoufia University. 279pp.
- El Habaak, G.H., (2001). A microorganism remains in the Proterozoic El-Dabbah Banded Iron Formation, Egypt. In: 2nd international conference on geology of Africa, Assiut, Egypt, vol 1, pp 79–99
- Kiyokawa, S., Suzuki, T., El-Dokouny, H. A., Dawoud, M., & Abuelhasan, M. M. (2020). Stratigraphy, petrology, and geochemistry of a Neoproterozoic banded iron sequence in the El-Dabbah Group, central Eastern Desert, Egypt. *Journal of African Earth Sciences*, 168, 103805
- Stern, R.J, Mukherjee, S.K., Miller, N.R., Ali, K., & Johnson, P.R., (2013). ~750 Ma banded iron formation from the Arabian-Nubian Shield: implications for understanding Neoproterozoic tectonics, volcanism, and climatic change. *Precam. Res* 239:79–94



Re-Os ISOTOPE RECORD IN THE PALEOCENE LIMESTONE OF THE CHICXULUB IMPACT BASIN

Honami Sato¹, Akira Ishikawa², Christopher M. Lowery³, Sean P.S. Gulick^{3,4,5}, Joanna V. Morgan⁶, and IODP-ICDP Expedition 364 Scientists

1. Department of Earth and Planetary Sciences, Kyushu University, Fukuoka, Japan
sato.honami.975@m.kyushu-u.ac.jp
2. Department of Earth and Planetary Sciences, Tokyo Institute of Technology, Tokyo, Japan
3. Institute for Geophysics, Jackson School of Geosciences, University of Texas at Austin, Austin, USA
4. Department of Geological Sciences, Jackson School of Geosciences, University of Texas at Austin, Austin, USA
5. Center for Planetary Systems Habitability, University of Texas at Austin, Austin, USA
6. Department of Earth Science and Engineering, Imperial College London, London, UK

1. Introduction

The impact event at the Cretaceous-Paleogene (K-Pg) boundary, ~66 million years ago, formed ~200-km diameter Chicxulub impact structure on the Yucatán Peninsula of the Gulf of Mexico (Gulick et al., 2008). The asteroid impact delivered osmium (Os) into the ocean, which records globally as a negative Os isotope (¹⁸⁷Os/¹⁸⁸Os) excursion in the pelagic carbonate sequences for ~200 thousand years (kyr) after the impact (Ravizza and VonderHaar, 2012). This impact-induced Os isotope excursion provides a unique means of constraining the time scale of recovery after the environmental perturbation. However, this approach has been established with the data from only three sites among the many reported the K-Pg boundary sections. Here we report new record of ¹⁸⁷Os/¹⁸⁸Os ratios and concentrations of highly siderophile elements (HSEs: Os, Ir, Ru, Pt, Pd, Re) in the earliest to middle Paleocene limestone deposited on top of the Chicxulub impact structure recovered during the IODP-ICDP Expedition 364 (Morgan et al., 2016).

2. Results

Age-corrected ¹⁸⁷Os/¹⁸⁸Os ratios are low in the earliest Paleocene limestone (~0.19) and then increase gradually. Subsequently, ¹⁸⁷Os/¹⁸⁸Os ratios recovered to steady state (~0.45) around ~2.5 million years (myr) after the impact. The ¹⁸⁷Os/¹⁸⁸Os ratios of the limestone within the Chicxulub impact basin are consistent with the values previously reported from the pelagic sites in that the ratios recover from low (~0.17 to 0.2) to steady state (~0.4) after the K-Pg impact (Ravizza et al., 2003; Ravizza and VonderHaar, 2012). Whereas the recovery time for Os isotope ratios is quite different. Although the ¹⁸⁷Os/¹⁸⁸Os values should recover on a time scale of ~200 kyr in the open ocean (Ravizza and VonderHaar, 2012), ¹⁸⁷Os/¹⁸⁸Os profile recorded in the impact basin remain lower than the expected values for at least the first ~1 myr of the Paleocene. The Os concentrations gradually decrease upward throughout the limestone. On the other hand, the high Ir concentrations at the base of the Paleocene

limestone (~0.49 ppb; Goderis et al., 2021) decrease abruptly, and then show almost constant values during the early to middle Paleocene limestone. The concentrations of HSE in the limestone samples exhibit depleted in Os-Ir-Ru and enriched in Pt-Pd-Re except for the base of the Paleocene limestone.

3. Discussion

Our results suggest that the Paleocene limestone accumulated in the Chicxulub impact structure recorded continuous but unique temporal evolution of seawater Os isotopic composition after the K-Pg impact, probably due to restricted connection to the global ocean. A possible mechanism to achieve the delayed recovery of ¹⁸⁷Os/¹⁸⁸Os values within the impact basin demands (1) only small influx of radiogenic Os in global seawater, and (2) a large input of unradiogenic Os from impact ejecta deposited in the Gulf of Mexico and on Yucatán Peninsula, or (3) input from the impact melt sheet underneath the central basin via venting of hydrothermal fluids.

References

- Gulick, S.P.S., Barton, P.J., Christeson, G.L., Morgan, J.V., McDonald, M., Mendoza-Cervantes, K., et al. (2008) Importance of pre-impact crustal structure for the asymmetry of the Chicxulub impact crater. *Nat. Geosci.* **1**, 131-135.
- Ravizza, G. and VonderHaar, D. (2012) A geochemical clock in earliest Paleogene pelagic carbonates based on the impact-induced Os isotope excursion at the Cretaceous-Paleogene boundary. *Paleoceanography* **27**, PA3219.
- Morgan, J.V., Gulick, S.P.S., Bralower, T., Chenot, E., Christeson, G., Claeys, P., et al. (2016) The formation of peak rings in large impact craters. *Science* **354**, 878-882.
- Ravizza, G. and Peucker-Ehrenbrink, B. (2003) Chemostratigraphic evidence of Deccan volcanism from the marine osmium isotope record. *Science* **302**, 1392-1395.
- Goderis, S., Sato, H., Ferrière, L., Schmitz, B., Burney, D., Kaskes, P., et al. (2004) Globally distributed iridium layer preserved within the Chicxulub impact structure. *Sci. Adv.* **7**, eabe3647.



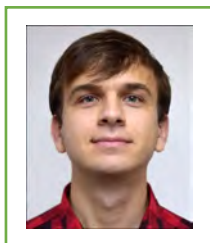
The geology of gold mineralization in the Nangodi greenstone belt, Ghana

Kwame Fynn¹, Axel Hofmann¹, Samuel Nunoo²

1. Department of Geology, University of Johannesburg, South Africa
paakwame100@gmail.com
2. Department of Earth Science, University of Ghana, Legon – Accra, Ghana

One of the recent gold discoveries in Ghana is the Namdini Gold Project in the northern part of the country situated within the Bole-Nangodi greenstone belt. The Bole-Nangodi greenstone belt consists of Birimian volcanic and volcanoclastic rocks (basalt to rhyolite) and immature sedimentary rocks (greywacke, shale) and is flanked on both sides by extensive granitoid complexes. Exploration in the area has led to the estimation of a 5.1 Moz ore reserve. We present petrographic analysis, whole rock major and trace element geochemistry and ore mineralogy and mineral chemistry of drill core from the Namdini Project. Gold mineralization is associated with

strongly sheared, volcanic arc-type meta-andesite and meta-dacite/-rhyolite. The mineralization is restricted to shear zones characterized by carbonate-quartz veins that acted as hydrothermal fluid pathways for the precipitation of sulphides hosting the gold. Compositional zoning in sulphides is interpreted as due to the evolution of mineralizing fluids from As-poor to As-rich, forming early-stage pyrite/arsenopyrite, followed by the deposition of As-poor, late-stage pyrite. Oriented sulphides, pressure shadows and deformed veins all suggest that the mineralization was coeval to the deformation of the Bole-Nangodi greenstone belt.



RARE EARTH ELEMENT ENRICHMENT OF THE LATE EDIACARAN KALYUS BEDS (SOUTHWESTERN BALTICA) THROUGH DIAGENETIC UPTAKE

Ion Francovschi¹, Eugen Grădinaru², Leonid Shumlyansky³, Relu D. Roban⁴, Mihai N. Ducea⁵, Valerian Ciobotaru⁶, Andrey Bekker⁷

1. University of Bucharest, Faculty of Geology and Geophysics, Bucharest, Romania
Institute of Geology and Seismology, Chişinău, Republic of Moldova

frankovski.ww@gmail.com

2. University of Bucharest, Faculty of Geology and Geophysics, Bucharest, Romania

3. Institute of Geological Sciences, Polish Academy of Sciences (ING PAN), Kraków, Poland
School of Earth and Planetary Sciences, Curtin University, Australia

4. University of Bucharest, Faculty of Geology and Geophysics, Bucharest, Romania

5. University of Bucharest, Faculty of Geology and Geophysics, Bucharest, Romania
Department of Geosciences, University of Arizona, Tucson, AZ, USA

6. Institute of Geology and Seismology, Chişinău, Republic of Moldova

7. Department of Earth & Planetary Sciences, University of California, Riverside, CA 92521, USA
Department of Geology, University of Johannesburg, Auckland Park 2006, South Africa

1. Introduction

The Kalyus Beds of the late Ediacaran Nagoryany Formation, Mohyliv-Podilsky Group, occurring in the northeastern part of the Republic of Moldova (southwestern Baltica) are dominated by black argillites with phosphorites and calcareous concretions [1, 2]. Four lithological groups were examined with respect to their rare earth element (REE), major and trace element geochemistry: phosphorites, enriched argillites, pure argillites and carbonate mounds.

2. Results and Discussion

Phosphorites and enriched argillites exhibit a pronounced middle-REE bulge suggesting a strong diagenetic uptake of REEs. Y/Ho ratios are mostly <35, values that are consistent with derivation of >90% of REEs from lithogenous sources. Pure argillites show a flat REE distribution similar to that of average upper continental crust (UCC), indicating that REEs are likely related to detrital siliciclastics derived from felsic to mafic source rocks of the adjacent regions of Baltica, which was isolated within paleo-oceans during the late Ediacaran. Carbonates show a light-REE depleted pattern with relatively high Y/Ho ratios (up to 53) that suggests the preservation of a predominantly hydrogenous (seawater derived) REE signal. Ce/Ce* ratios of ~0.80–1.02 reflect suboxic to anoxic seawater conditions. This is a locally and temporally constrained anoxic event, since widespread oxic conditions were specific for the continental margins of Baltica. The phosphorites and enriched argillites groups of the Kalyus Beds show high middle-REE enrichment comparable to those of other known world phosphorite deposits. The MREE hat-shaped pattern was most probably acquired at greater burial depths during late diagenesis.

within the Ukrainian Shield (c. 1980–2100 Ma), the Korosten anorthosite-mangerite-charnockite-granite complex in the northwestern region of the Ukrainian Shield (c. 1780 Ma), and the large Mazury anorthosite-mangerite-charnockite-granite complex in northeastern Poland (c. 1499–1548 Ma) were source rocks for the Kalyus Beds.

Their total REE contents are high (793–1735 ppm) and are of potential economic interest. These results provide insights for expanding global REE exploration targets and may have implications for a better understanding of the depositional environments during the late Ediacaran.

References

- Velikanov, V.A., Aseeva, E.A., Fedonkin, M.A., 1983. *Vendian of Ukraine*. Naukova Dumka, Kiev, 1–161 (in Russian).
- Bukatchuk, P.D., Bliuk, I.B., Pokatilov, V.P., 1988. *Geological map of the Moldavian Soviet Socialist Republic, scale 1:200 000*. Explanatory notes. Moldovageology, Chişinău, 1–273 (in Russian).

Geochronological analyses on detrital zircons indicate that the Paleoproterozoic granitoids widely distributed

Understanding Multistage Syntectonic Iron Ore Hypogene Mineralization in the São Francisco craton – A Textural Approach

Carlos A. Rosière^{1,*}, Leonardo E. Lagoeiro², Flavia C. Silveira Braga¹,
Ricardo Pagung de Carvalho³

1.CPMT/Department of Geology, Univ. Federal de Minas Gerais, 31270-901 Belo Horizonte, Minas Gerais, Brazil

2.CME/ Geology Department, Universidade Federal do Paraná, Curitiba, Paraná, Brazil

3.Graduate School, IGC, Universidade Federal de Minas Gerais, 31270-901 Belo Horizonte, Minas Gerais, Brazil

*Corresponding author: crosiere@gmail.com

Keywords: Hypogene iron mineralization, EBSD petrofabric analysis, Sao Francisco craton.

Large-scale mineralization events associated with two orogenies generated economically important IF-hosted hypogene high-grade iron orebodies in the Brazilian São Francisco craton each with distinctive fabric and chemical characteristics as genetic diagnostic features. During the ca. 2.1-2.0 Ga Transamazonian orogeny, magnetite-martite-hematite massive to banded orebodies from the Quadrilátero Ferrífero District in Minas Gerais are controlled by thin-skinned tectonic structures. The age of mineralization is estimated from the upper intercept of a concordia plot from Monazite grains intergrown with hematite that delivered the date of 2038.2 ± 6.6 Ma (Th-Pb SHRIMP). Metamorphic fluids promoted leaching of gangue minerals and substitution of carbonates in the Paleoproterozoic Cauê Iron Formation of the Minas Supergroup to form irregularly shaped orebodies that mimetizes the structure of the iron formation or massive veins that may cut across the overlying country rocks. The age of the Cauê IF is bracketed by the U-Pb SHRIMP date of 2580 ± 7 Ma for the youngest detrital zircons from the underlying quartzites and the Pb-Pb isochron date of 2420 ± 19 Ma for the overlying dolostones. A manifold mineralization scenario is envisioned during the Ediacaran to Cambrian Brasiliano orogeny. Modified hydrothermal fluids of magmatic and metamorphic origin recurrently mineralized the Archean to Paleoproterozoic terranes of the cratonic core including the Cauê IF, the younger, carbonate-free IFs of the Serra da Serpentina Group (1990 ± 16 Ma - MDA, U-Pb SHRIMP date), and the post-Rhyacian sequences of the lower Espinhaço Supergroup along five events with ages of 497, 508, 518, 526, and 536 Ma related to granitic intrusions with the development of far-field hydrothermal alteration. Episodic circulation of hot fluids is likely to have been driven by seismic pumping from the Araçuaí-West Congo orogen (AWC). The syntectonic mineralization phase is characterized by pressure solution and leaching of gangue minerals

and deformation and crystallization of hematite with the development of tabular to linear shaped orebodies displaying a crystallographic preferred orientation (CPO) in thrust fault-related shear zones. During a late to post-tectonic phase massive Ti- and Mn-rich magnetite orebodies from the Guanhões Tectonic Block crystallized at the contact zone of anatectic pegmatite intrusions in deep to intermediate crustal level.

Petrofabric studies undergone in the schistose orebodies reveal a complex interplay of crystal-plastic deformation and solution-precipitation and grain growth during syntectonic mineralization under upper greenschist facies conditions. Strain-dependent diffusion processes including anisotropic growth of oriented specularite plates in shear zones likely overprinted early deformational features but did not obliterate the crystallographic preferred orientation.

References

- Aguilar, C. et al. Palaeoproterozoic assembly of the São Francisco craton, SE Brazil: new insights from U-Pb titanite and monazite dating. *Precambrian Res.* 289:95–115. 2017.
- Alkmim, F. F. et al.: The Araçuaí belt. In: Heilbron, M. et al. (eds.) *The São Francisco craton, eastern Brazil (Regional Geology Reviews)*, pp. 255–276, Springer, Heidelberg (2017).
- Babinski, M. et al.: The Pb/Pb age of the Minas Supergroup carbonate rocks, Quadrilátero Ferrífero, Brazil. *Precambrian Res.* 72, 235–245 (1995).
- Ferreira, F. et al: Texture development during progressive deformation of hematite aggregates: Constraints from VPSC models and naturally deformed iron oxides from Minas Gerais, Brazil. *J. Struct. Geol.* 90, 111-127 (2016)
- Hartmann, L. A. et al.: Provenance and age delimitation of Quadrilátero Ferrífero sandstones based on zircon U-Pb isotopes. *J. S. Am. Earth Sci.* 20, 273–285 (2006).

-
- Rolim, V. K. et al. The Orosirian-Statherian banded iron formation-bearing sequences of the southern border of the Espinhaço Range, Southeast Brazil. *J. S. Am. Earth Sci.* 65:43–66. (2016)
- Rosière, C.A., et al.: Microstructures, textures and deformation mechanisms in hematite. *J. Struct. Geol.* 23(9), 1429-1440m(2001).
- Rosière, C. A., and Rios, F. J.: The origin of hematite in high-grade iron ores based in infrared microscopy and fluid inclusion studies: the example of the Conceição Deposit, Quadrilátero Ferrífero, Brazil. *Econ.Geol.* 99(3), 611–624 (2004).
- Rosière, C. A. et al.: The itabirite from the Quadrilátero Ferrífero and related high-grade ores: an overview. *Rev. Econ. Geol.* 15, 223–254 (2008).
- Rosière, C. A. et al.: Domanial fabrics of hematite in schistose shear zone-hosted high-grade Fe ores: the product of the interplay between deformation and mineralization. *J. Struct. Geol.* 55, 150–166 (2013).
- Silveira Braga, F. C. et al.: 2020. Ediacaran-Cambrian far-field hydrothermal event in the southeast of the São Francisco craton, Brazil: evidence from zircon U-Pb SHRIMP, trace elements, Lu-Hf and oxygen isotopes. *Lithos.* 356–357:1-2.105365 (2020)



Phosphorous cycle on the Archean Earth: geological constraints

Takeshi Kakegawa

Department of science, University of Tohoku, Sendai, Japan

kakegawa@tohoku.ac.jp

1. Introduction

Phosphorous cycle on the early Earth has been debated for last decades. On the other hand, it has been uncertain concerning about the source and speciation of phosphorous and sink mechanisms in the cycles. The points of debates were (1) source of phosphorous for origin of life and early life, (2) speciation of phosphorous in hydrosphere, and (3) their abundances.

2. Results and discussion

Geochemical and mineralogical studies were performed on Archean submarine volcanic rocks and banded iron formations from Pilbara (3.4 Ga), Barberton (3.2 Ga) and Abitibi and Wawa (2.7 Ga). The examined basalts and rhyolites were suffered from submarine hydrothermal alteration and seafloor CO₂ metasomatism. They contained various secondary apatite and monazite with extremely rare phosphides. This observation and thermodynamic calculations indicate that phosphate was a dominant specie in the migrating fluids, rather than reduced phosphorous species. Altered volcanic rocks are in general depleted in phosphorous concentrations. These findings suggest that Archean oceanic crusts behaved as the source of phosphorous in the global phosphorous cycle.

The some BIFs (3.2 Ga and 2.7 Ga) were found to be rich in phosphate (up to 0.8 wt%), accompanied with occurrences of large sulfur-bearing apatite. Such high phosphorous concentrations and apatite chemistry cannot be caused by adsorption-enrichment model by Fe-(hydro) oxides. Close association of P enrichments and organic matter in the examined samples suggest the P accumulation in BIFs through sedimentary organic matter. Those results indicate that microbial processes had a significant role to sink phosphate on Archean sea floor.

References

Kakegawa, T., Noda, M. and Nannri, H (2002) Geochemical cycles of bio-essential elements on the early Earth and their relationships to origin of life. *Resource geology*, 52, 83–89.

Rasmussen, B., Muhling, J.R., Suvorova, A. and Fischer, W.W. (2021) Apatite nanoparticles in 3.46–2.46 Ga iron formations: Evidence for phosphorus-rich hydrothermal plumes on early Earth. *Geology*, 49, 647–651.

Reinhard, C.T., Planavsky, N.J., Gill, B.C., Ozaki, K., Robbins, L.J., Lyons, T.W., Fischer, W.W., Wang, C., Cole, D.B. and Konhauser, K.O. (2017) Evolution of the global phosphorus cycle. *Nature*, 484, 498–501.



Paleontological and geochemical fingerprints of Iron-Oxidizing Bacteria from the ca. 1.88 Ga Gibraltar Granular Iron Formation

Alex Kovalick¹, Andrey Bekker¹, Andrew Heard², Nicolas Dauphas²

¹University of California, Riverside

²Woods Hole Oceanographic institute

³The University of Chicago

Introduction

Most major Iron Formations (IFs) were deposited before the Great Oxidation Episode¹. However, after >500 Myr, shallow-water Granular Iron Formations (GIFs) appear on multiple, disconnected cratons at ca. 1.88 Ga¹. Several GIFs have been dated at ca. 1.88 Ga and linked to high Fe flux from submarine, high-temperature, hydrothermal activity associated with Large Igneous Province emplacement¹. Redox-sensitive Rare Earth Elements (REE) indicate Fe-oxyhydroxide precipitation at the redoxcline^{2,3}. Fe-oxidation is thought to be biological,

either oxygen production via photosynthesis or iron oxidation by microaerophilic Iron-Oxidizing Bacteria (IOB)^{4,5}. Although microfossils from stromatolites in these GIFs have been linked to biological Fe-oxidation^{3,4,5}, their exact biological affinity remains uncertain. We present a combined paleontological and geochemical study of GIFs from the ca. 1.88 Ga Gibraltar Formation (Slave craton) with special attention to microfossil-bearing Fe-rich stromatolites to develop a clearer picture of the microbial ecosystems driving GIF deposition.

Results & Discussion

Samples from the Gibraltar Formation were analyzed for major and trace elements, including REE contents and Fe-isotope ($\delta^{56}\text{Fe}$) values. Redox proxies indicate non-quantitative Fe-oxidation at the redoxcline. Based on the highest measured $\delta^{56}\text{Fe}$ value in GIF samples of +0.73‰ and an oxidation-related Fe-isotope fractionation factor of $\epsilon=1.5\%$ ⁶, the upper bound for the $\delta^{56}\text{Fe}$ value of $\text{Fe}^{2+}_{(\text{aq})}$ can be constrained to -0.78‰, consistent with $\delta^{56}\text{Fe}$ values from submarine high-temperature hydrothermal sources⁷, further supported by positive Eu anomalies. A large range of bulk $\delta^{56}\text{Fe}$ values from +0.73‰ to -0.58‰ reflects the expression of Rayleigh fractionation associated with varying degree of partial oxidation of $\text{Fe}^{2+}_{(\text{aq})}$ rather than quantitative Fe-oxidation via cyanobacterial oxygen production.

(West Australia) formations. Significantly, filamentous microfossils bear closer resemblance to the modern IOB, *Mariprofundus Ferrooxydans*, than those found in other ca. 1.88 Ga GIFs. $\delta^{56}\text{Fe}$ values of individual stromatolite lamina (+0.35‰ to +0.63‰) are isotopically heavier than most measured whole-rock samples, consistent with non-quantitative Fe-oxidation. This significant difference between whole-rock and stromatolite lamina markedly contrast with Fe-rich stromatolites from the 2.46-2.43 Ga Griquatown GIF of South Africa. Based on a small range in Fe-isotope values for both the Griquatown GIF whole-rock and stromatolite lamina, it was argued that $\text{Fe}^{2+}_{(\text{aq})}$ was quantitatively sequestered from seawater with oxygen produced by cyanobacteria living in stromatolites⁸. To date, these new paleontological and geochemical results for the Gibraltar GIF are the strongest evidence for IOB driving Fe-oxidation in Paleoproterozoic GIFs, fingerprinting the signature of partial biological Fe-oxidation in ca. 1.88 Ga tidal settings.

Fe-rich stromatolites contain microfossil morphotypes in the Gibraltar Formation similar to those found in the ca. 1.88 Ga Gunflint (Canada) and Frere

References

1. Bekker, A., et al. Iron Formations: Their Origins and Implications for Ancient Seawater Chemistry. in *Treatise on Geochemistry* 9, 561–628 (Elsevier, 2014).
2. Planavsky, N., et al. Rare earth element and yttrium compositions of Archean and Paleoproterozoic Fe formations revisited: new perspectives on the significance and mechanisms of deposition. *Geochimica et Cosmochimica Acta* 74.22, 6387-6405 (2010).
3. Planavsky, N., et al. Iron-oxidizing microbial ecosystems thrived in late Paleoproterozoic redox-stratified oceans. *Earth and Planetary Science Letters* 286, 230–242 (2009).
4. Barghoorn, E., and Tyler, A. Microorganisms from the Gunflint Chert. *Science* 147.3658, 563- 575 (1965).
5. Cloud, P. Significance of the Gunflint (Precambrian) Microflora. *Science* 148.3666, 27-35 (1965).
6. Johnson, C., Beard, B., Weyer, S., Chapter 3 in "Fe Isotope Fractionation Factors: Biological Experiments." *Iron Geochemistry: An Isotopic Perspective*. Edited by Hoefs, J., Springer, 65-84 (2020).
7. Rouxel, O., et al. Biogeochemical cycling of iron isotopes at Loihi Seamount. *Eos Transactions* 88, 52-52 (2007).
8. Heard, A., et al. production and rapid iron oxidation in stromatolites immediately predating the Great Oxidation Event. *Earth Planet. Sci. Lett.* 582, 117416 (2022).



Hf-W dating of ancient zircon using a NanoSIMS

Yuji Sano

Center for Advanced Marine Core Research, Kochi University, Nankoku,
Kochi 783-85 02, Japan. yuji.sano@kochi-u.ac.jp

1. Introduction

Two types of methods are known for measuring the formation age of rocks and minerals. The first is based on radioactive decay of nuclides with long half-lives comparable to the age of the earth, such as ^{238}U - ^{206}Pb system (Schoene, 2014). The second is based on the use of extinct nuclides that were once present but have now been reduced to undetectable amounts by radioactive decay, such as the ^{26}Al - ^{26}Mg (Davis and McKeegan, 2014) and ^{129}I - ^{129}Xe (Jeffrey and Reynolds, 1961) systems. The former method has been applied to the formation of continental crust, great volcanic activity, and various other geological phenomena, while the latter method has been applied to samples from the early solar system such as primitive meteorites and Hadean earth (before 4 billion years ago). In this study, we report recent results of the ^{182}Hf - ^{182}W ages of ancient zircon minerals using a NanoSIMS.

2. Experiments

We selected a zircon mineral located in the silicate portion of mesosiderite (Asuka882023), a type of lithic iron meteorite that differentiated about 4.6 billion years ago. As earth samples, zircon minerals extracted from sedimentary rocks collected in the Jack Hills region of Western Australia were used. The latter is known to exhibit a wide range of ages from about 3 billion to 4.4 billion years (Wilde et al., 2001). In this study, samples older than 3.8 billion years were initially selected by a simple laser ablation-ICP mass spectrometer. Selected zircon samples were polished to a mirror finishing before gold coat. All dating was performed using a high lateral resolution secondary ion mass spectrometer (NanoSIMS50) installed at the Atmosphere and Ocean Research Institute, University of Tokyo. First, a primary oxygen ion beam of approximately 7 μm in diameter was focused on the surface, and the emitted zirconium, uranium, and lead isotope ions were measured at a mass resolution of 4,000 (Takahata et al., 2008). The same ion beam was then used to measure zirconium, hafnium, and tungsten isotopes with a mass resolution increased to 10,000 (Koike et al., 2017).

3. Results and Discussion

The ^{238}U - ^{206}Pb and ^{207}Pb - ^{206}Pb ages of the mesosiderite (Asuka882023) zircon are 4375 ± 150 Ma (1σ) and 4502 ± 38 Ma (1σ), respectively. On the other hand, absolute ages cannot be obtained from dating method using extinct nuclides, but relative ages are derived

from the difference in slope on an isochron diagram. In order to convert this to a formation age, it is necessary to analyze a sample with a known absolute age, called an anchor, under the same conditions. In this study, zircon isolated from the Agout meteorite, which is considered to be crustal material of the asteroid Vesta and classified as basaltic eucrite, was used as the anchor. The ^{207}Pb - ^{206}Pb age is reported precisely at 4554.5 Ma (Iizuka et al., 2015). On the $^{180}\text{Hf}/^{186}\text{W}$ - $^{182}\text{W}/^{186}\text{W}$ isochron, the anchor exhibits a slope of $^{182}\text{W}/^{180}\text{Hf} = 3.1 \pm 0.7 \times 10^{-5}$. On the other hand, mesosiderite exhibited a slope of $6.67 \pm 3.70 \times 10^{-6}$. The relative age obtained from the difference in slopes is $+21.7^{+5.7}_{-10.4}$ Ma (1σ). Therefore, the absolute age of Asuka882023 was determined to be $4532.8^{+5.7}_{-10.4}$ Ma (1σ). The same work as for the mesosiderite zircon is being done for the Jack Hills zircon, and the details will be presented at the meeting.

References

- Davis, A.M., and MaKeegan, K.D. (2014) Short-lived radionuclides and early solar system chronology. *In Treatise on Geochemistry*, **Volume 1**, 361-395.
- Iizuka, T., Yamaguchi, A., Haba, K., Amelin, Y., Holden, P., Zink, M., Huyskens, M.H., Ireland, T.R. (2015) Timing of global crustal metamorphism on Vesta as revealed by high-precision U-Pb dating and trace element chemistry of eucrite zircon. *Earth Planet. Sci. Lett.* **409**, 182-192.
- Jeffery, P.M., and Reynolds, J.H. (1961) Origin of excess ^{129}Xe in stone meteorites. *J. Geophys. Res.* **66**, 3582-3583.
- Koike, M., Sugiura, N., Takahata, N., Ishida, A., and Sano, Y. (2017) U-Pb and Hf-W dating of young zircon in mesosiderite Asuka 882023 *Geophys. Res. Lett.* **44**, 1251-1259.
- Schoene, B. (2014) U-Th-Pb Geochronology. *In Treatise on Geochemistry*, **Volume 3**, 341-378.
- Takahata, N., Tsutsumi, Y., and Sano, Y. (2008) Ion microprobe U-Pb dating of zircon with a 15 micrometer spatial resolution using NanoSIMS. *Gondwana Res.* **14**, 587-596.
- Wilde, S.A., Vallye, J.W., Peck, W.H., and Graham, C.M. (2001) Evidence from detrital zircons for the existence of continental crust and oceans on the Earth 4.4 Gyr ago. *Nature* **409**, 175-178.



Archaean geology of the Singhbhum Craton, India: Insights from greenstone belts and cratonic cover sequences.

Jaganmoy Jodder^{1, 2*}, Axel Hofmann², Marlina Elburg², Hanqiang Xie³ and Pierre Durand²

1. Evolutionary Studies Institute, University of the Witwatersrand, South Africa.

jaganmoyj@gmail.com, Pierre.Durand@wits.ac.za

2. Department of Geology, University of Johannesburg, South Africa.

ahofmann@uj.ac.za, marlinae@uj.ac.za

3. Beijing SHRIMP Center, Chinese Academy of Geological Sciences,

26 Baiwanzhuang Road, Beijing 100037, China. rock@bjshrimp.cn

1. Introduction

In recent times, the Archaean geological record of the Singhbhum Craton has been investigated in detail regarding early Earth crustal processes, tectonics, magmatic-detrital zircon geochronology, early life research, and Fe-Mn mineralization associated with volcano-sedimentary successions. However, many of these studies are hampered by a lack of a basic stratigraphic framework of the various litho-stratigraphic units, complicating our understanding of the overall Archaean geology of the Singhbhum Craton. Here, we share new insights on the Palaeoarchaean greenstone belts and Meso-Neoarchaean intracontinental volcano-sedimentary sequence of the Singhbhum Craton.

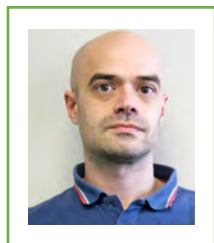
2. Results

New magmatic zircon U-Pb ages determined from the felsic volcanic rocks of Badampahar supracrustals are represented by their crystallization age at c. 3.51 Ga. Intrusive granitoids/trondhjemitic sills exposed in the Daitari and Gorumahisani belts yielded inherited zircon ages of 3.58, 3.55, 3.51 Ga and their crystallization ages around 3.38, 3.37, 3.35 and 3.29 Ga respectively. Deep-water turbidites reported from the upper part of the Badampahar Group in the Daitari area provided detrital U-Pb zircon ages of 3.53 Ga and 3.51 Ga, which are indistinguishable from the underlying felsic volcanic rocks in the Daitari belt. Intrusive granitoid within iron formation of the Gorumahisani greenstone belt provided an age of c. 3.29 Ga. Detrital zircon age data recovered from the Koira Group sandstones yielded peak population clusters around 3.3, 3.2, 3.0, 2.9 and 2.8 Ga respectively with the youngest recognizable detrital population of <2.7 Ga from an event horizon intercalated within iron formation. This puts the microbial structures from the Palaeoarchaean record of the Daitari belt, and the stromatolites of Neoarchaeon age from the Koira Group in a better temporal frame.

3. Discussion

The Palaeoarchaean to Neoarchaeon record of the Singhbhum Craton provides us with a vital window to evaluate how distinctive suites of volcano-sedimentary rocks that belong to a specific geodynamic setting

and/or geological processes operated during the Archaean. We demonstrate that Palaeoarchaeon greenstones exposed in the northern and southern parts of the Singhbhum Craton consists of largely submarine mafic-ultramafic volcanic rocks interlayered with minor felsic volcanic rocks and chemical sedimentary rocks. In contrast, the Meso-Neoarchaeon intracontinental volcano-sedimentary succession of Koira Group preserved in the western part of the Singhbhum Craton is predominantly made up of shallow-marine sandstones, associated with sub-aerial mafic volcanic rocks, iron formation with rare occurrence of stromatolites. Importantly, the ca. 3.51 Ga felsic volcanic rocks from the Palaeoarchaeon supracrustals of the Badampahar Group in the Singhbhum Craton permit comparison with co-eval felsic volcanic units reported from the lower part of the Onverwacht, Nondweni, Warrawoona groups of the Kaapvaal and Pilbara cratons. Otherwise, widespread sub-aerial volcanism is noted from the Meso-Neoarchaeon record of the Koira, Dominion-Pongola, Ventersdorp and Fortescue groups that likely reflect the presence of Large Igneous Provinces (LIPs) in the abovementioned cratons and/or a global phenomenon likely linked to mantle overturning event during Meso-Neoarchaeon times. Occurrence of stromatolites from the Neoarchaeon record of the Koira Group, and possible microbial structures from older greenstones indicate that microbial activity was widespread during the Archaean in the Singhbhum Craton.



Trace element and S-isotope composition of pyrite from the Witwatersrand Basin, South Africa

Andrea Agangi¹, Axel Hofmann², Giuliana da Costa², Emilie Thomassot³

1. Akita University, Akita, 010-8502, Japan
andrea_agangi@gipc.akita-u.ac.jp
2. University of Johannesburg, Auckland Park, 2006, South Africa
ahofmann@uj.ac.za, giulianavcosta@terra.com.br
3. Université de Lorraine, Vandœuvre les Nancy, 54500, France
Emilie.thomassot@univ-lorraine.fr

1. Introduction

The Mesoarchaeon Witwatersrand Basin of South Africa hosts the largest Au fields ever discovered, having produced in excess of 53000 t of Au since its discovery in 1886 (Frimmel, 2019). The gold is hosted by thin (cm- to dm-scale), laterally extensive quartz-pyrite conglomerates that mark large-scale unconformities that formed after the emergence of the Kaapvaal Craton, following its consolidation at around 3.1 Ga. The Witwatersrand Basin is here defined in a broad sense, as including the largely volcanic ca. 2.96 Ga Dominion Group, the ca. 2.95 – 2.80 Ga Witwatersrand Supergroup (itself composed of the shale-dominated West Rand Group and the sandstone-dominated West Rand Group), and the ca. 2.79 – 2.68 Ga Ventersdorp Supergroup (Gumsley et al., 2020; Paprika et al., 2021), thus spanning some 0.3 Ga.

Despite their unique size and gold content, the Witwatersrand deposits have equivalents spanning in age from the Mesoarchaeon to the Palaeoproterozoic, such as the Neoarchaeon Fortescue Group of Western Australia (Spinks et al., 2021) and the Palaeoproterozoic Huronian Supergroup (Ulrich et al., 2011). Therefore, genetic models developed for the Witwatersrand can potentially be applied to other deposits worldwide. Following a long-standing discussion centred on paleoplacer- and hydrothermal-related mechanisms, recent models for the formation of the Witwatersrand deposits involve mobilisation of gold from the hinterland through leaching by an acidic meteoric water and deposition in fluvial-coastal areas, a model that appears to remove the need of a particularly Au-rich source rock, and has implications on the atmospheric conditions at the time of formation.

2. Results and discussion

The auriferous Witwatersrand conglomerates contain abundant quartz and pyrite, in addition to a large number of heavy minerals, such as zircon, rutile and chromite. Textural observations indicate that pyrite is largely detrital in origin, a feature considered to reflect oxygen-poor atmospheric compositions of the Archaeon and early Palaeoproterozoic, although epigenetic pyrite is also commonly observed. We compiled previous and new textural observations, in-situ elemental analyses and multiple-S isotope analyses of pyrite to infer the conditions of formation

and the implications on the sedimentary-diagenetic environments and the gold-forming conditions.

The wide range of textures, elemental and isotopic compositions of detrital pyrite reflect the variety of sediment sources. In addition, special inclusion-rich pyrite grains and grain fragments that have delicate textures suggesting short transport and local derivation, are interpreted as reflecting the proximal environment near the site of final deposition. Strong zoning observed in some grains (with detrital cores and overgrowths) reflects the conditions of formation of syngenetic to epigenetic pyrite, with increases of metals such as Ni and As in overgrowths. S-isotope analyses indicate an overall relatively large range of $\delta^{34}\text{S}$ (-10 to +21 ‰), allowing for local formation via sulfate reduction. The modest mass-independent S-isotope variations ($\Delta^{33}\text{S} = -1.5$ to +1.7 ‰), and the data scatter in a $\delta^{34}\text{S}$ vs $\Delta^{33}\text{S}$ plot, so that the data do not follow the common positive trend found in other Archaeon successions (the Archaeon Reference Array), seems to reflect a trend observed for the Mesoarchaeon.

References

- Frimmel, H. E., 2019, The Witwatersrand basin and its gold deposits, in Kröner, A., and Hofmann, A., eds., *The Archean geology of the Kaapvaal craton, Southern Africa*: Springer, p. 325–345.
- Gumsley, L., et al., 2020, Neoarchean large igneous provinces on the Kaapvaal Craton in southern Africa re-define the formation of the Ventersdorp Supergroup and its temporal equivalents. *Geological Society of America Bulletin*, 132 (9-10): 1829–1844.
- Paprika, D., et al., 2021, Age of the Dominion-Nsuze Igneous Province, the first intracratonic Igneous Province of the Kaapvaal Craton. *Precambrian Research*, 363, 106335.
- Spinks, S. C., et al., 2020, The Neoarchean Conglomerate-Hosted Gold of the West Pilbara Craton, Western Australia, *Economic Geology*, 116, 629-650.
- Ulrich, T., Long, D. G. F., Kamber, B. S., Whitehouse, M. J., 2011, In situ trace element and sulfur isotope analysis of pyrite in a Paleoproterozoic gold placer deposit, Pardo and Clement Townships, Ontario, Canada, *Economic Geology*, 106, 667-686.



RAPID RECOVERY OF STRONTIUM ISOTOPE COMPOSITIONS IN THE OCEAN AFTER THE END-CRETACEOUS ASTEROID IMPACT (IODP EXP. 364 "CHICXULUB IMPACT CRATER")

Kosei E. Yamaguchi¹, Kohta Mutoh¹, and Tsuyoshi Ishikawa²

1. Department of Chemistry, Toho University, Chiba, Japan

kosei@chem.sci.toho-u.ac.jp

2. Kochi Institute for Core Sample Research, JAMSTEC, Kochi, Japan

t-ishik@jamstec.go.jp

1. Introduction

End-Cretaceous mass extinction was most likely triggered by an impact of a ~10km-diameter asteroid that created ~180-km-diameter Chicxulub impact crater off Yucatán Peninsula, Mexico. In early 2016, IODP Exp. 364 drilled into the offshore portion of the crater and successfully recovered a long core from 506 to 1,335m below seafloor, intersecting the K-Pg boundary, at ~100% recovery (Morgan et al., 2016). This record offers critical insights into the environmental effects of the impact and the cratering process (e.g., Lowery et al. 2018; Riller et al. 2018; Gulick et al., 2019; Kring et al. 2020; Goderis et al. 2021).

During the cratering process, massive amount of crustal materials (granitoids) were fractured, fluidized, solidified (Riller et al. 2018), and extensively leached by hydrothermal alteration (Kring et al. 2020). Geochemical cycles of elements in the ocean were disturbed by the above processes, but questions remain as to (1) how much and what kind of toxic elements (heavy metals) were released into the ocean, (2) how their elemental concentrations in the ocean were modified and recovered, (3) the time-scale of the recovery processes. In order to find clues for the questions raised above, we focused on the geochemical behaviors of Sr in the ocean.

Post-impact sedimentary rocks (carbonates and marlstones) recovered by the IODP Exp. 364 were used in this study for high-resolution analysis. They are mixtures of detrital materials by continental weathering and oceanic carbonates with varying mixing ratios. A 10% acetic acid was used to selectively leach the carbonate-fraction, which presumably reflects oceanic Sr. The oceanic Sr was purified and concentrated using multi-step ion exchange chromatography, and analyzed its isotope compositions using TIMS at Kochi Core Center.

2. Results and Discussion

A rapid increase in the ⁸⁷Sr/⁸⁶Sr ratios right after the K-Pg impact was observed, using the samples that filled the crater with high sedimentation rates (Gulick

et al., 2019). This suggests instantaneous and massive release of crustal materials into the ocean upon impact. After the abrupt increase, the time series Sr isotope record gradually approached, taking ~10⁶ years, the world-average curve proposed by McArthur et al. (2001).

However, an unexpected and intriguing spike (positive excursion) was observed at several millions years after the K-Pg impact. Analytical artefact is considered highly unlikely because silicate (clay) fractions having continental high ⁸⁷Sr/⁸⁶Sr ratios are not leached by 10% acetic acid, and, if any, quantitatively very difficult to induce spike-like modifications of low ⁸⁷Sr/⁸⁶Sr ratios representing major carbonate fraction. Therefore, here we consider a very rapid (possibly local) increase of oceanic ⁸⁷Sr/⁸⁶Sr ratios due to rapid input of high ⁸⁷Sr/⁸⁶Sr continental materials from, for example, mega-earthquakes and/or volcanic activities. Recently, Nicholson et al. (2022) proposed the Nadir impact structure off Guinea Terrace, suggested by seismic images, was potentially coeval to the Chicxulub impact crater. Although the radiometric dating is missing for the Nadir "crater", we may have geochemically detected, for the first time, the Sr isotope excursion induced by the Nadir impact event.

In the presentation, we present a model based on a simple mass balance calculation to estimate the amount of Sr released from altered crustal materials upon asteroid impact, or the volume of the crustal materials that experienced intensive hydrothermal alteration.

References

- Goderis et al. (2021) *Sci. Adv.* **7**, eabe3657.
- Gulick, S.P.S. et al. (2019) *PNAS* **116**, 19342–19351.
- Kring, D.A. et al. (2020) *Sci. Adv.* **6**, eaaz3053.
- Lowery, C.M. et al. (2018) *Nature* **558**, 288–291.
- McArthur et al. (2001) *J. Geology* **109**, 155–170.
- Morgan, J.V. et al. (2016) *Science* **354**, 878–882.
- Mutoh, K. (2022) *Master's thesis*. Toho University.
- Nicholson, U. et al. (2022) *Sci. Adv.* **8**, eabn3096.
- Riller, U. et al. (2018) *Nature* **562**, 511–518.

Are the diamictites from the Eastern Desert of Egypt represent glacial deposits??? The regional and the global distribution and the paleoclimatic significance during the pan-African time

Mai El-Lithy

Geology Department, Faculty of Science, Menoufia University, Egypt

maielleithy24@gmail.com

Formation of the Arabian-Nubian Shield (ANS) and the East African Orogen (EAO) took place between 1000–525 Ma (Robinson et al., 2014). ANS crustal growth encompassed a time of dramatic climatic change, articulated as the Snowball Earth hypothesis (SEH). SEH identifies tremendous paleoclimatic fluctuations during Neoproterozoic time. Sedimentary units in the Eastern Desert of Egypt and NW Saudi Arabia may record evidence of the Sturtian Snowball Earth event in the northernmost ANS. The studying of the paleogeology, inherited elements and paleoclimatology including the "Snowball Earth" in the Arabian-Nubian shield is rather new and upraising topic (e.g. Miller et al., 2003; Stern et al., 2006; Stern et al., 2011, El-Dokouny 2017).

The Neoproterozoic diamictite in Egypt is exposed in the Central Eastern Desert between 26°N and 22°N. Only there are four small (only few to several kilometers across) localities of the Neoproterozoic diamictite are known till now (East of Gabal Atud area, Wadi Kariem area, Wadi Mobarak area, and Muweilih area); (Akaad and Essawy 1965). In some localities diamictite is associated with BIF. The paleoenvironment, paleoclimatology, and origin of this diamictite is still controversial up to now. It is thought that this diamictite represent glacial deposits (Stern et al., 2006; Ali et al., 2010; Stern et al., 2011); however much more field investigations, petrographical, geochemical and age dating data are needed to reach the aim and ascertain this statement. The Neoproterozoic diamictite in the Eastern Desert (and the correlative Nuwaybah, Northern Saudi Arabia) deposition age is about 750 Ma or slightly later about 700- 720 Ma (Li et al., 2018), consistent with being deposited during the Sturtian glaciation (~740–660 Ma). New ideas concerning the nature, geological processes, tectonic setting and origin of the clasts from diamictites in east Atud are innovated and evidenced by El-Lithy (in preparation). The Paleoproterozoic and Neoproterozoic clasts have no known source within the ensimatic Arabian–Nubian Shield. The distribution of the pre-Neoproterozoic ages is like the distribution of the pre-Neoproterozoic ages in Yemen and Saharan Metacraton suggesting that these clasts have been transported hundreds of kilometers, may be by ice-rafting (Ali et al., 2010). Neoproterozoic diamictite and its environs have been

chosen to be our target to test the idea; we thought that those rocks seem to be promising to verify the SHE in the Eastern Desert, Egypt as a part of the Arabian-Nubian shield.

References

- Akaad, M.K., and Essawy, M.A., (1965). Petrography, origin and sedimentation of the Atud Formation and its bearing on the early part of the geological history of the basement complex of the Eastern Desert of Egypt. *Bull. Sci. and Tech. Assiut*, 8, 75-102.
- Ali et al., 2010. Neoproterozoic diamictite in the Eastern Desert of Egypt and Northern Saudi Arabia: evidence of ~750 Ma glaciation in the Arabian–Nubian Shield? *Int J Earth Sci (Geol Rundsch)* (2010) 99:705–726.
- El-Dokouny, H.A., 2017,. Geochemical and isotopic studies of some Neoproterozoic banded iron formations from the Eastern Desert of Egypt: insights into 'snowball earth' seafloor environments. PhD Thesis, Menoufiya University, Egypt. 279 pp.
- El-Lithy, M.A., (In Preparation). The Atud diamictite rocks in the Eastern Desert of Egypt: Implications for the paleogeological processes and paleoclimatology. PhD Thesis, Menoufiya University, Egypt.
- Li et al., 2018. Old continental crust underlying juvenile oceanic arc: Evidence from northern Arabian-Nubian Shield, Egypt. *AGU100. Advancing Earth and Space Science. Geo. Res. Lett.*, 45,7, p. 3001-3008.
- Miller et al., 2003,. Significance of the Tambien Group (Tigray, N. Ethiopia) for Snowball Earth events in the Arabian-Nubian Shield. *Precambrian Res.* 121, 263–283.
- Robinson et al., 2014,. Arabian shield magmatic cycles and their relationship with Gondwana assembly: Insights from zircon U-Pb and Hf isotopes. *Earth and Planetary Science Letters*;408: 207-225.
- Stern et al., 2006,. Evidence for the Snowball Earth hypothesis in the Arabian–Nubian Shield and the east African Orogen. *J Afr Earth Sci* 44:1–20
- Stern et al., 2011. Evidence for early and mid-cryogenian glaciation in the Northern Arabian-Nubian Shield (Egypt, Sudan, and western Arabia). *Geological Society Memoir*, 36(1), 277–284



Geochemistry and Tectonic Setting of Metavolcanic Rocks from the Cape Three Points Area in the Southern Ashanti Paleoproterozoic Birimian Greenstone Belt, Ghana

Kwabina Ibrahim^{1*}, Marian Selorm Sapah¹, Frank K. Nyame¹, Johnson Manu¹, Thomas M. Akabzaa¹, Patrick A. Sakyi¹, George M. Tetteh², Satoshi Yoshimaru³, Shoichi Kiyokawa³, Takashi Ito⁴

1. Department of Earth Science, Faculty of Science, University of Ghana, P. O. Box LG 58, Legon, Accra, Ghana
2. University of Mines and Technology, Tarkwa, Ghana.
3. Department of Earth and Planetary Sciences, Kyushu University, Fukuoka, Japan.
4. Ibaraki University, Mito, Japan.

* Corresponding author (email: Kwabina.ibrahim@gmail.com)

Major and trace element data of metavolcanic rocks from the Cape Three Points area in the southern Ashanti Paleoproterozoic Birimian greenstone belt of Ghana were studied to determine geochemical characteristics and infer a possible tectonic setting of the rocks. Textural and mineralogical features identifiable in outcrops as well as in hand samples and under the microscope indicate they are dark grey to grey, massive to pillowed, moderately deformed and dominantly metabasalt rocks characterized by SiO₂ contents from 57.10- 65.54 wt.%, TiO₂ 0.74-0.86 wt.%, Al₂O₃ 12.13-17.09 wt.%, Fe₂O₃ (total Fe) 7.21-10.35, MgO 3.74-7.65 wt.% and CaO 4.84-

6.30 wt.%. Trace element contents vary widely, as in Cr from 219 to 509 ppm, V from 112 to 225 ppm, Ni 76.6 to 123.0 ppm, Cu 18.50 to 88.32 ppm and Zn 25.93 to 103 ppm. The rocks display flat to moderately fractionated REE patterns with some samples distinctly characterized by strongly negative to no Eu anomalies present. Chondrite normalised multi-element diagrams show that the rocks are enriched in LILE relative to HFSE and in LREE relative to HREE. The geochemical signatures of the rocks generally suggest they formed in a subduction-related setting with some degree of sub-lithospheric contamination.



Paleoenvironmental changes off Antarctic Peninsula during last 5,000 years

Minoru Ikehara¹, Kodai Kato², Yuji Kato³ and Osamu Seki⁴

1. Center for Advanced Marine Core Research, Kochi University, Kochi, Japan
ikehara@kochi-u.ac.jp
2. Graduate School of Integrated Arts and Sciences, Kochi University, Kochi, Japan
3. Faculty of Life and Environmental Sciences, University of Tsukuba, Ibaraki, Japan
4. Institute of Low Temperature Science, Hokkaido University, Sapporo, Japan

1. Introduction

The Antarctic Ice Sheet (AIS) is a large body of freshwater, and its variation is a dominant factor in global sea-level change and atmospheric meridional circulation. Therefore, it is extremely important to understand the AIS mass change in response to global warming. The Antarctic Peninsula (AP) is one of the fastest-warming regions on Earth (Turner et al., 2005), and ice sheet melting over the past 50 years has been enhanced (Cook et al., 2005). However, these satellite records are limited to the past half-century, so the actual climate change and ice sheet melting on a long timescale have not been elucidated. In this study, we investigated a piston core KH-19-6-PC01 taken from the Western Bransfield Basin bundle, which is formed by giant ice streams from the AP (Canals et al., 2000) to reveal the paleoenvironment changes of the northwestern AP over the past 5,000 years.

2. Results and discussions

During the middle Holocene warm period from 5000 to 3200 years, multiple increasing events with abundant iceberg rafted debris (IBRD) and fossil chrysophyte cysts were found, and compound-specific hydrogen isotopes of fatty acid biomarkers also showed an increased glacial meltwater input in this area. These findings suggest that the Antarctic Peninsula ice sheet (APIS) significantly melted during the mid-Holocene. Based on organic carbon and Br content, and diatom abundance, there was also a significant increase in biological production in this area. During this period, a La Niña mode developed in the tropics (Moy et al., 2002; Conroy et al., 2008), the Amundsen Sea Low was enhanced, and the Southern Annular Mode (SAM) showed positive anomalies (Moreno et al., 2018), indicating that the teleconnection with SAM+ may have accelerated APIS melting by amplifying local meridional wind anomalies around the AP, which enhanced warm air advection from lower latitudes to the AP. On the other hand, after about 3200 years, the IBRD decreased and biological production declined, suggesting that ice sheet melting decreased with the development of the El Niño mode.

References

- Canals, M., Urgeles, R., Calafat, A.M. (2000) Deep seafloor evidence of past ice streams off the Antarctic Peninsula. *Geology* **28**, 31-34.
- Conroy, J.L., Overpeck, J.T., Cole, J.E., Shanahan, T.M., Steinitz-Kannan, M. (2008) Holocene changes in eastern tropical Pacific climate inferred from a Galápagos lake sediment record. *Quaternary Science Reviews* **27**, 1166-1180.
- Cook, A. J., Fox, A. J., Vaughan, D. G., and Ferrigno, J. G., (2005) Retreating Glacier Fronts on the Antarctic Peninsula over the Past Half-Century. *Science*, **308**, 541-544.
- Moreno, P.I., Vilanova, I., Villa-Martínez, R., Dunbar, R.B., Mucciarone, D.A., Kaplan, M.R., Garreaud, R.D., Rojas, M., Moy, C.M., De Pol-Holz, R., Lambert, F. (2018) Onset and Evolution of Southern Annular Mode-Like Changes at Centennial Timescale. *Scientific Reports* **8**, 3458.
- Moy, C.M., Seltzer, G.O., Rodbell, D.T., Anderson, D.M. (2002) Variability of El Niño/Southern Oscillation activity at millennial timescales during the Holocene epoch. *Nature* **420**, 162-165.
- Turner, J., Colwell, S. R., Marshall, G. J., Lachlan-Cope, T. A., Carleton, A. M., Jones, P. D., Lagun, V., Reid, P. A., and Iagovkina, S. (2005) Antarctic climate change during the last 50 years. *International Journal of Climatology*, **25**, 279-294.



A REVIEW: AGE DETERMINATION METHODS OF MARINE MANGANESE DEPOSITS

Takashi Ito¹

1. Ibaraki University, Mito, Japan.

1. Introduction

Marine manganese nodules and crusts are ubiquitous on the current deep-sea floor within the circumspect of vertically well-mixed oceanic milieu. There is growing recognition of manganese crust as a valuable repository that records a plethora of palaeoceanographic, geochemical, and palaeoenvironmental data (Hein et al., 1992; Frank, 2002; Klemm et al., 2005; Usui et al., 2007; Nielsen et al., 2009).

While numerous techniques have been employed for determining the age of marine manganese deposits, each approach boasts its own strengths and limitations. This study briefly introduces the characteristics of each dating method.

2. Biostratigraphy

The biostratigraphy of micro- or nannofossil molds is one of the methods for direct dating (e.g. Harada and Nishida, 1976; Cowen et al., 1993). This method, however, has a disadvantage due to its limited application to manganese oxides of shallow seamount areas above calcium carbonate compensation depth (CCD). In addition, it may contain reworked fossils, so applying it in combination with other methods is desirable.

3. ¹⁰Be Method

¹⁰Be method has been widely applied for the estimation of the growth rate (e.g. Segl et al., 1984, 1989; Usui et al., 2007). This method is applicable for manganese nodules and crusts younger than ca. 15 Ma, based on the relatively short half-life. In principle, the older the age, the greater the analytical error.

4. Sr isotope stratigraphy

Sr isotope stratigraphy has been considered as an applicable dating method for manganese crusts with growth histories exceeding 20 Ma (Futa et al., 1988, Ingram et al., 1990). Later, it was pointed out that Sr in the growth layer was exchangeable with seawater Sr during the growth process (VonderHaar et al., 1995). Evaluation as a dating tool has not yet been completed.

As another application example of Sr isotope stratigraphy, Ito et al. (1998) suggested that the buried nodules in DSDP/ODP cores are in situ fossil deposits from the past deep-sea floor during the Cretaceous to Quaternary periods.

5. Os isotope stratigraphy

During the past two decades, Os isotope stratigraphy has been going up the frequency as the

dating method for manganese crust. Klemm et al. (2005) showed long-term growth with hiatuses from the latest Cretaceous to the present for the single thick manganese crust from the central Pacific. On the other hand, another age model without hiatuses was proposed for the identical manganese crust (Nielsen et al., 2009). The accuracy of this method will be improved by adding other dating data and detailed observation of growth structures. In addition, the age determination without for the periods showing drastically Os isotopic excursions (datum points such as the Eocene-Oligocene and Cretaceous-Paleogene boundaries) requires caution.

6. Magnetostratigraphy

Recently, magnetostratigraphy is also applying the dating of marine manganese crusts (Oda et al., 2011, Yuan et al., 2017). This method has the advantage of being applicable to a wide age range. However, since it only obtains a positive magnetization-reverse magnetization pattern, its reliability increases by comparing it with other methods. For example, Oda et al. (2011) attempted a comparison with the ¹⁰Be method.

References

- Cowen, J. P. et al. (1993) *Mar. Geol.* **115**, 289-306.
 Futa, K., et al. (1988) *Geochim. Cosmochim. Acta* **52**, 2229-2233.
 Harada, K. and Nishida, S. (1976) *Nature* **260**, 770-771.
 Hein, J. R. et al. (1992) *Paleoceanography* **7**, 63-77.
 Hyeong, K. et al. (2013) *Palaeogeogr., Palaeoclimatol., Palaeoecol.*, **392**, 293-301.
 Ingram, B. L. et al. (1990) *Geochim. Cosmochim. Acta* **54**, 1709-1721.
 Ito, T. et al. (1998) *Geochim. Cosmochim. Acta* **62**, 1545-1554.
 Klemm, V. et al. (2005) *Earth Planet. Sci. Lett.*, **238**, 42-48.
 Ku, T. L. et al. (1982) *Nature* **299**, 240-242.
 Nielsen, S. G. et al. (2009) *Earth Planet. Sci. Lett.*, **278**, 297-307.
 Segl, M. et al. (1984) *Nature* **309**, 540-543.
 Segl, M. et al. (1989) *Paleoceanography* **4**, 511-530.
 Usui, A. et al. (2007) *Island Arc*, **16**(3), 420-430.
 VonderHaar, D. L. et al. (1995) *Geochim. Cosmochim. Acta* **59**, 4267-4277.
 Yuan, W. et al. (2017). *Scientific Reports*, **7**(1), 16748.

Occurrence and Geological Setting of a Neoproterozoic Ironstone in the Buem Structural Unit (BSU), Ghana

David Y. Kumah*¹, Frank Awuah¹, Daniel Boamah¹, F. K. Nyame²

1. Ghana Geological Survey Authority, Accra, Ghana

2. Department of Earth Science, University of Ghana, Legon, Accra

*Corresponding Author: kumahadinkrahdaavid@gmail.com

Recent geological mapping by the Ghana Geological Survey Authority within the metacratonic Buem Structural Unit in the southeastern part of Ghana revealed the occurrence of iron-rich rocks within a general succession of basal sandstone, shale, cherty carbonate, chert, ironstone and sandstone. Some of these rocks are, in places, associated with serpentinitised mafic/ultramafic bodies. Well preserved and obviously primary iron-rich rocks generally occur as grey to dark grey, massive to well bedded or banded units traceable for tens of kilometres along

strike. Individual bands display variable thickness on the cm scale. The alternating iron and silica rich layers especially present in jaspilitic samples look similar to Rapitan BIF. In general, highly weathered supergene-derived or enriched iron ore overlies the primary material in many areas of outcrop. The occurrence, field relations and general petrographic features, especially the presence in some outcrops of what appears to be "diamictic" features, suggest the ironstone may be closely related to glacial diamictites of the Neoproterozoic or Sturtian snowball earth events.



CHAOTIC BEDS IN THE PALEOGENE MUROTO FORMATION AT MUROTO PENINSULA, KOCHI PREFECTURE, JAPAN

Hinako Matsumoto¹, Satoshi Tonai²

1. Department of Science and Technology, University of Kochi
b22m6g62@s.kochi-u.ac.jp

2. Department of Science and Technology, University of Kochi
s-tonai@kochi-u.ac.jp

1. Introduction

The upper Eocene to lower Oligocene Muroto Formation exposed on the Muroto Peninsula, Kochi Prefecture, Japan, was deposited in a plate convergence zone. The Muroto Formation is characterized by many chaotic layers and sand injected rocks (Taira et al., 1980; Taira, 1984), which are thought to have been formed by deformation of sediments in the shallow submarine zone. Deformation that occurs in the shallow subsurface of plate convergence zones reflects the conditions of the convergence zone (e.g., Festa et al., 2022). Therefore, their frequency, distribution, formation process, and causes constrain the picture of the plate convergence region in the southwest Japan Arc, including Shikoku. Subduction of the Philippine Sea Plate off Shikoku is considered to have started in the Early to Middle Miocene (Taira, 1984), and the Nankai Trough off Shikoku is considered to have been subducted by another plate earlier. Information on the state of the subduction zone at that time is limited (e.g., DiTullio and Byrne, 1990), and it is expected that the process and environment in which the chaotic layers were created will provide constraints. In this study, field surveys were conducted at Gyotomisaki Beach, Muroto City, Kochi Prefecture, where the Muroto Formation is continuously exposed over a wide area, in order to clarify the formation process of the Muroto Formation based on the distribution and internal structure of the chaotic layers and sand injected rock layers.

2. Results

The formation in the area is about 220 m thick, trends NE–SW, dips to the northwest at more than 60°, and is younging to northeastward. The strata were classified into seven lithology mainly based on the ratio of sandstone and mudstone and the deformation characteristics. In addition, some of these lithology show a certain sequence which is characterized mainly by the sandy mudstone layer at the bottom and the clastic injectite layer at the top. This sequence is the chaotic sequence. Layer shortening faults, which seem to have been originally as thrusts, are developed in the lower-middle part, and layer extension faults, which seem to have been originally as normal faults, are developed in the upper part. The shear direction

based on the folds and thrusts in the chaotic sequence is parallel to the paleocurrent direction inferred from the sole marks on the bottom of the sandstone. Total nine chaotic sequences were recognized in the study area. The individual thickness is about 1–25 m, accounting for 40% of the total layer thickness in the study area.

3. Discussion

The chaotic sequences have the following characteristics. (1) They show a certain succession, although some parts are lacking, (2) Some deformed structures exhibiting extension and shortening parallel to the bedding plane, which were formed when the strata were unconsolidated, and (3) Sand injectites were formed at the same time as the deformation of the sequence, based on their distribution and cross-cutting relationships. (4) The chaotic sequences are cut by tectonic faults through the study area. Based on these characteristics, the chaotic sequences were considered to be formed by a submarine landslide. During the transport, the sandy mudstone bed at the base was mainly sheared, the strain decreased in the upper part, and the upper alternation of sandstone and shale hardly deformed. The direction of landslide movement estimated from the deformation structure in the chaotic sequences was parallel to the paleocurrent direction indicated by the surrounding strata.

References

- DiTullio, L. and Byrne, T., 1990, Deformation paths in the shallow levels of an accretionary prism: The Eocene Shimanto Belt of southwest Japan. *Geol. Soc. Amer. Bull.*, **102**, 1420–1438.
- Festa, A., Barbero, E., Remitti, F., Ogata, K. and Pini, G. A., 2022, Mélanges and chaotic rock units: Implications for exhumed subduction complexes and orogenic belts. *Geosystems and Geoenvironment*, **1**, 100030.
- Taira, T., Tashiro, M., Okamura, M. and Katto, J., 1980, The geology of the Shimanto Belt in Kochi Prefecture, Shikoku, Japan. *Selected Papers in Honor of Prof. Jiro Katto, Geology and Paleontology of the Shimanto Belt*, 319–389 (in Japanese).
- Taira, A., 1984, Tectonic significance of sandstone dikes in the Eocene Muroto Group, Shimanto Belt (subduction complex), Shikoku. *Res. Rep. Kochi Univ., Nat. Sci.*, **32**, 161–178.



In situ sulfur isotope analysis of sulfide in >3.95 Ga metasedimentary rocks: Sulfur cycling and microbial activity in the Eoarchean

Ryota Mihori^{1*}, Yusuke Sawaki¹, Masahiro Kayama¹, Takayuki Ushikubo², Kenji Shimizu² and Tsuyoshi Komiya¹

1: Department of Earth Science and Astronomy, Graduate School of Arts and Sciences, The University of Tokyo, Tokyo 153-8902, Japan

2: Kochi Institute for Core Sample Research, Japan Agency for Marine-Earth Science and Technology (JAMSTEC), Kochi 783-8502, Japan

*Corresponding author: mihori-ryota@g.ecc.u-tokyo.ac.jp

1. Introduction

Origin and early evolution of life are very important issues among earth science. Existence of early life itself have been demonstrated by presence of ¹²C-rich carbon from metasedimentary rocks in the Eoarchean (e.g., Rosing, 1999). However, it is still ambiguous what kinds of metabolism and ecosystems were established in the early earth.

Although sulfur-metabolism is considered as one of the oldest metabolisms from a biological viewpoint (Wagner et al., 1998), there is no geochemical evidence such as sulfur isotopes of sulfide for the sulfur-metabolism until ca. 3.5 Ga (Shen et al., 2001; Shen et al., 2009). Previous studies investigated sulfur isotopes of sulfide mainly from banded iron formation (BIF) and clastic sedimentary rocks in the Isua supracrustal belt to find the evidence, but it is still ambiguous. Therefore, it is necessary to make more comprehensive investigation of sulfide from various host rocks in other geologic terrains.

We focus on the Nulliak supracrustal rocks in Saglek Block, northern Labrador, Canada. They consist of metamorphic rocks originating from chert, BIF, carbonate rocks, pelite, and conglomerate, which date back to 3.95 Ga (Shimojo et al., 2016). The metamorphic grades are estimated to be Amphibolite to Granulite facies for Big Island, SJHE, and SJHS, whereas Granulite facies for Shuldham Island and Pangertok Inlet. ¹²C-rich graphite indicating existence of early life was found there (Tashiro et al., 2017).

2. Results

Sulfide minerals exist in all types of metasedimentary rocks. The pelitic rocks tend to contain more sulfides, some of which coexist with graphite, whereas the BIFs have few sulfides. The sulfides in chert are relatively large, up to several hundreds of micrometers in size, and most of them have euhedral to subhedral forms. SEM-EDS analysis indicates two types of sulfides, namely pyrite and pyrrhotite, but most of them are pyrrhotite. The pyrites have peaks around 340 and 380 cm⁻¹ on the Raman spectra, whereas the pyrrhotites have peaks around either 170, 340 or 380 cm⁻¹ on the spectra. Their Raman spectra also support two types of sulfides. The pyrites exist in all types of

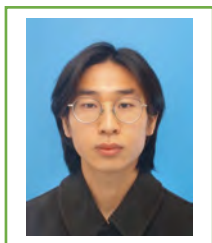
metasedimentary rocks except for BIF, and most of them are surrounding by magnetite-rims. Some pyrrhotites are associated with pentlandite or chalcopyrite. All host rocks but cherts contain pyrites only in the low-grade metamorphic areas. Only cherts contain pyrites even in the Pangertok Inlet.

3. Discussion

It is well known that transition from pyrite to pyrrhotite occur during metamorphism. Given that pyrite is stable up to 743 °C, occurrence of both pyrite and pyrrhotite in the low-grade metamorphic areas (~740 °C) and only pyrrhotite in high-grade areas (~800 °C), except for those in cherts, indicates that the pyrrhotites was formed from the pyrites by desulfidation during the metamorphism.

References

- Rosing, M.T. (1999) ¹³C-Depleted carbon microparticles in >3700-Ma sea-floor sedimentary rocks from West Greenland. *Science* **283**, 674-676.
- Wagner, M., Roger, A.J., Flax, J.L., Brusseau, G.A., and Stahl, D.A. (1998) Phylogeny of dissimilatory sulfite reductases supports an early origin of sulfate respiration. *J Bacteriol.* **180**, 2975-2982.
- Shen, Y., Buick, R., and Canfield, D. E. (2001) Isotopic evidence for microbial sulphate reduction in the early Archaean era. *Nature* **410**, 77-81.
- Shen, Y., Farquhar, J., Masterson, A., Kaufman, A.J. and Buick, R. (2009) Evaluating the role of microbial sulfate reduction in the early Archean using quadruple isotope systematics. *Earth Planet. Sci. Lett.* **279**, 383-391.
- Shimojo, M., Yamamoto, S., Sakata, S., Yokoyama, T.D., Maki, K., Sawaki, Y., Ishikawa, A., Aoki, K., Aoki, S., Koshida, K., Tashiro, T., Hirata, T., Collerson, K.D., and Komiya, T. (2016) Occurrence and geochronology of the Eoarchean, ~3.9 Ga, Iqaluk Gneiss in the Saglek Block, northern Labrador, Canada: Evidence for the oldest supracrustal rocks in the world. *Precamb. Res.* **278**, 218-243.
- Tashiro, T., Ishida, A., Hori, M., Igisu, M., Koike, M., Méjean, P., Takahata, N., Sano, Y. and Komiya, T. (2017) Early trace of life from 3.95 Ga sedimentary rocks in Labrador, Canada. *Nature* **549**, 516-518.



IN-SITU ANALYSIS OF CARBONATE-ASSOCIATED PHOSPHATE: IMPLICATIONS FOR SECULAR CHANGE OF SEAWATER PHOSPHATE THROUGH THE PRECAMBRIAN

Ryosuke Nagao^{1*}, Satoshi Yoshida², Yuki Ishihara¹, Yusuke Sawaki², Yuta Ijichi³, Takeshi Ohno⁴, Yuichiro Ueno⁵, Takafumi Hirata³, Tsuyoshi Komiya²

*corresponding author: ryo101112@g.ecc.u-tokyo.ac.jp

1. Department of Earth and Planetary Science, Graduate School of Science, The University of Tokyo, Bunkyo-ku, Japan
2. Department of Earth Science and Astronomy, Graduate School of Arts and Sciences, The University of Tokyo, Tokyo 153-8902, Japan
3. Geochemical Research Center, The University of Tokyo, Tokyo 113-0033, Japan
4. Department of Chemistry, Faculty of Science, Gakushuin University, Mejiro 1-5-1, Toshima-ku, Tokyo, 171-8588, Japan
5. Department of Earth and Planetary Sciences, Tokyo Institute of Technology, 2-12-1 Ookayama, Meguro-ku, Tokyo 152-8551, Japan

1. Introduction

Phosphorus is one of the most crucial bio-essential and bio-limiting elements and has a significant influence on the redox state of the earth's biosphere. It has been widely accepted that oxygenic photosynthesis may have emerged at least before the great oxidation event (GOE), but it is also considered that the Precambrian biosphere remained anoxic. This led to the proposal that the Precambrian primary productivity was severely limited by the low dissolved inorganic phosphate (DIP) levels through the Precambrian [1].

Shimura et al. 2014 [2] first proposed that the P contents in carbonate minerals can be used as a paleo-DIP proxy and showed that the seawater was enriched in Phosphate after the Marinoan glaciation. Recent works also validate that the P contents of carbonate minerals (termed carbonate-associated phosphate, or CAP), are a useful proxy [3-4]. Ingalls et al. 2022 [4] conducted whole-rock analysis by acid digestion for CAP in Neoproterozoic, but the data are highly scattered possibly due to the influence of minor clastic contamination and recrystallization. To avoid the effect of contaminations, we conducted an *in-situ* analysis of the carbonates using fs LA-ICP-MS at the Geochemical Research Center, the University of Tokyo, Japan. In this study, we present measured CAP/(Ca+Mg) ratios from late Archean to Phanerozoic shallow marine stromatolitic carbonates.

2. Results

Measured P/(Ca+Mg) ratios range from 0.03 to 1.10 mmol/mol in Neoproterozoic Tumbiana Formation, Western Australia; from 0.05 to 0.16 mmol/mol in Paleoproterozoic Duck Creek Formation, Western Australia; from 0.01 to 0.59 mmol/mol in Midproterozoic Khoraidi Formation, Nepal.

3. Discussion

We checked the time profiles of signal intensities of ICP-MS to detect the sign of contamination and exclude these data for a CAP comparison.

Secular change of CAP/(Ca+Mg) ratios shows that the Precambrian CAP contents tend to be larger than the contemporary counterpart. High to moderate CAP contents in Precambrian carbonates suggests that the DIP in the Precambrian Ocean was not scarce as previously suggested [1]. The apparent contradiction between the early emergence of oxygenic photosynthesis and the delayed rise of atmospheric P_{o2} should be reconciled by other explanations.

References

- [1] L. A. Derry, "Causes and consequences of mid-Proterozoic anoxia," *Geophys Res Lett*, vol. 42, no. 20, pp. 8538–8546, 2015, doi: <https://doi.org/10.1002/2015GL065333>.
- [2] T. Shimura et al., "In-situ analyses of phosphorus contents of carbonate minerals: Reconstruction of phosphorus contents of seawater from the Ediacaran to early Cambrian," *Gondwana Research*, vol. 25, no. 3, pp. 1090–1107, 2014, doi: 10.1016/j.gr.2013.08.001.
- [3] M. S. Dodd et al., "Development of carbonate-associated phosphate (CAP) as a proxy for reconstructing ancient ocean phosphate levels," *Geochim Cosmochim Acta*, vol. 301, pp. 48–69, May 2021, doi: 10.1016/j.gca.2021.02.038.
- [4] M. Ingalls, J. P. Grotzinger, T. Present, B. Rasmussen, and W. W. Fischer, "Carbonate-Associated Phosphate (CAP) Indicates Elevated Phosphate Availability in Neoproterozoic Shallow Marine Environments," *Geophys Res Lett*, vol. 49, no. 6, p. e2022GL098100, 2022, doi: <https://doi.org/10.1029/2022GL098100>.



The restoration of sedimentary environment of mudstone sequences in Goto Group, Nagasaki Prefecture, Japan

Hiroaki Takahashi¹, Shoichi Kiyokawa¹, Masaru Yasunaga²,
Yuta Ikebata³, Minoru Ikehara⁴

1. Kyushu university
2. Goto city office, Goto Islands Geopark promotion group
3. DIA CONSULTANTS CO., Ltd.
4. Kochi university

1. Introduction

The Goto Islands are located at the westernmost tip of the Japan archipelago and preserve a lower to middle Miocene sedimentary sequences, which is related to opening of the Sea of Japan. The Goto Groups was deposited around 22-15 Ma, and its detailed stratigraphy and structure have recently been clarified (Kiyokawa et al., 2022). The lower unit consists of thin greenish volcanoclastic rocks. The middle units consists of alternating sandstones and shales in lacustrine and meandering fluvial environments. The upper unit consists of thick sandstones of fluvial-deltaic facies. In the Goto Groups, where detailed studies of the structural development have been conducted, we decided to reconstruct the sedimentary field (lakes, flood plains, etc.) of the shale layers. In addition, to determine the origin of carbon, we conducted TOC analysis and carbon stable isotope ratio measurement to clarify the stratigraphic changes.

2. Methods

We identified the depositional sites of the mudstone layers containing organic matter by root mapping/detailed columnar map/facies analysis and observed the evolution of the mudstone layers from the lower to the upper part of the Goto Formation. Thin sections were then prepared from the collected mudstones and characterized for constituent minerals and black organic matter using optical and electron microscopy. Eighty bulk mudstone samples were dried and ground, and after carbonate removal with 6NHCl, organic carbon concentration (TOC) and carbon stable isotope ratios were measured at the Kochi Core Center using an elemental analyzer FlashEA1112 (ThermoFisher).

3. Results

- The lower unit (Kayaba-ura) consists of 20-50 cm of volcanoclastic debris, which becomes finer-grained toward the top of the unit and develops parallel lobes. Volcanoclastic debris is interbedded with mudstone several tens of cm thick, with TOC of 0.25% and $\delta^{13}C$ of -25.1‰.
- The lower part of the middle unit (Togi) consists of thick mudstone-winning sandstone-mudstone alternation, with 5-10 cm alternation regularly

repeated and interbedded with thin sandstone layers. Some ripple marks are developed in the sandstone layers; TOC is 0.02% and $\delta^{13}C$ is -24.1‰.

- The upper part of the central unit (Toraku) consists of sandstone-mudstone alternation with ripples and regional stratigraphy. Three-dimensional channel structures and cutbank structures with lag breccias are prominent in the sandstone layers. The thick sandstone layer is interbedded with a 50 cm thick mudstone layer. The mudstone layer is distributed outside the cutbank and is not interbedded with the sandstone layer, suggesting that it is a floodplain deposit. TOC is 0.17% and $\delta^{13}C$ is -24.7‰.

- Lower part of upper unit (Uchiori). Three upper fine-grained intervals of transition from 5-10 m thick sandstone to 50 cm-1 m thick mudstone were observed; TOC was 0.57% and $\delta^{13}C$ was -25.5‰.

- The lower part of the upper unit (Toyanokubi) consists of sandstone-mudstone alternation with ϵ -type stratigraphy and is more than 10 m thick. The TOC and $\delta^{13}C$ values are 0.47% and -28.9‰, respectively.

4. Discussion

The origin of organic matter in lake sediments are plankton, aquatic plants, and terrestrial plants, and their carbon isotopic compositions are -30‰, -21‰, and -27‰, respectively (Pearson and Coplen, 1978). Land plants are divided into C3 and C4 plants based on their photosynthetic circuits (Vander Merwe, 1982). C3 plants prefer low temperature and humid environments, and their $\delta^{13}C$ values are low in the range of -21 to -35‰. On the other hand, C4 plants prefer high temperature environments and have high $\delta^{13}C$ values ranging from -6‰ to -19‰. These results suggest that the organic matter in the mudstones of the Goto Group is derived from C3 plants.

5. Conclusion

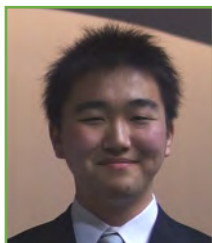
The organic carbon concentration in the mudstones of the Goto Group is 0.2%, and the stable isotope ratio of carbon is around -25‰. The organic carbon

concentration in the mudstone beds of the Goto Group is 0.2%, and the carbon stable isotope ratio is around -25‰.

References

- Pearson, F.J.Jr. and Coplen, T.B., 1978: Stable isotopes in lakes (translated by Yoshihiko Mizutani). In: The Science of the Lakes. Translated by Mineo Okuda and Nobuhiko Handa, Kokin shoin, 508p. (Original title: Lakes, Lerman, A. ed., Springer Verlag, New York)
- Shoichi Kiyokawa et al., 2022, Stratigraphic reconstruction of the lower-middle Miocene Goto Group, Nagasaki Prefecture, Japan, Islands arc, p.1-76.
- Yoshiro Ueda, 1961, A study of the Goto group. Kyushu University Institutional Repository, vol.5, p.51-61
- Van der Merwe, N. J., 1982: Carbon isotopes, photosynthesis and archaeology. *Am. Sci.*, 70, 596-606
- Masaru Yasunaga, Shoichi Kiyokawa, and Kazuhiro Uemura, 2007, Lithostratigraphy of the Neogene Goto Group and plant megafossils in Wakamatsu-jima and Nakadori-jima, central part of Goto islands, Nagasaki Prefecture. *Journal of the Sedimentological Society of Japan*, no.64, p.151-161

Behavior of phosphorous during the 2.7 Ga submarine hydrothermal activities at Abitibi Greenstone Belt, Canada



Yuki Takashina¹, Akizumi Ishida¹, and Takeshi Kakegawa¹

1. Department of Earth Science, Tohoku University, Sendai, Japan

yuki.takashina.p3@dc.tohoku.ac.jp

ishidaz@tohoku.ac.jp

kakegawa@tohoku.ac.jp

1. Introduction

Phosphorus is an essential element for life. The chemical specie of phosphorus is phosphate on the modern Earth, and most likely for Archean Earth. Weathering of continental rocks is the dominant source of phosphate in hydrosphere and biosphere of the modern Earth. On the other hand, the mass of continents is considered to be very small in the Archean age. This leads to the hypothesis of phosphate-poor environments in Archean hydrosphere and biosphere (e.g., Reinhard et al. 2017). Leaching of phosphate from Archean oceanic basalts by submarine hydrothermal alteration has been proposed as an alternative process to supply phosphate into hydrosphere and then to biosphere (Kakegawa et al., 2002; Rasmussen et al., 2021). Although this hypothesis has many advantages, direct evidence has not yet been obtained. Clarification of the behavior of phosphorus due to hydrothermal activity in the Archean is expected to lead to a more advanced understanding of phosphorous cycle on the early Earth.

Therefore, the purpose of the present study is set to examine the behavior of phosphorus in pillow lava samples in the Archean during hydrothermal alteration of the seafloor. 2.7 Ga pillow lavas and hyaloclastites from the Abitibi Greenstone Belt in Canada were examined in the present study. The pillow lava was separated into core and rim portions, and mineralogical and geochemical studies were performed separately.

2. Results

Veins of apatite and sphene were found only in the rim portion. Those veins were formed by migration of phosphorous and titanium in examined rocks and always associated with carbonate veins or carbonation alteration. This suggests that leaching and migration of phosphorous and titanium were caused by carbonate-rich hydrothermal fluids.

It is found that the sphene veins formed at the edge of the volcanic glass and was not associated with carbonate minerals. Those observation and mineralogical assemblages suggest the following sequence of alteration: (1) early hydration of volcanic

glasses, (2) later carbonation of buried and hydrated pillow lavas followed by (3) metamorphic overprint.

Major and trace element analyses were performed on the examined samples. Rim portions of pillow lavas, in general, enriched in Ti, Fe, Mg, Ca, V, Sr, Rb, Ba and P. Those enrichment trends are consistent with mineral assemblages.

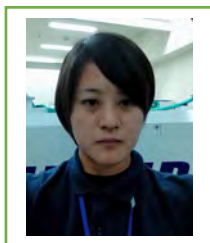
Carbon isotope compositions of carbonate are implying that the sources of CO₂ to form calcite were magmatic and atmospheric. Sulfur isotope compositions of sulfides yield relatively homogeneous compositions. This suggests that reduction of seawater sulfate did not occur within the pillow lavas. Instead, H₂S, which has homogeneous δ³⁴S values, were introduced into pillow lavas from outer systems.

3. Discussion

This study revealed that carbonate-rich hydrothermal fluids can migrate and concentrate phosphorus and titanium. A part of phosphorous and titanium was most likely released into seawater by discharge of the hydrothermal fluids. The behavior of phosphorus due to submarine hydrothermal activity during the Precambrian age is still not fully understood. The results of this study are expected to provide new insights into the problem of the origin of phosphorus during the Archean.

References

- Kakegawa, T., Noda, M. and Nannri, H (2002) Geochemical cycles of bio-essential elements on the early Earth and their relationships to origin of life. *Resource geology*, 52, 83–89.
- Rasmussen, B., Muhling, J.R., Suvorova, A. and Fischer, W.W. (2021) Apatite nanoparticles in 3.46–2.46 Ga iron formations: Evidence for phosphorus-rich hydrothermal plumes on early Earth. *Geology*, 49, 647–651.
- Reinhard, C.T., Planavsky, N.J., Gill, B.C., Ozaki, K., Robbins, L.J., Lyons, T.W., Fischer, W.W., Wang, C., Cole, D.B. and Konhauser, K.O. (2017) Evolution of the global phosphorus cycle. *Nature*, 484, 498–501.



U-Pb geochronology and geochemistry in zircon of the Utsubo granitic pluton, Hida Belt, central Japan

Mami Takehara¹ and Kenji Horie^{1,2}

1. SHRIMP Laboratory, National Institute of Polar Research, 10-3, Midori-cho, Tachikawa-shi, Tokyo 190-8518, Japan

Takehara.mami@nipr.ac.jp

2. Department of Polar Sciences, The Graduate University for Advanced Studies (SOKENDAI), Japan

1. Introduction

Geochronology with the chemical evolution of magmas is an essential consideration in the growth of continental crust. A zoned pluton provides an excellent opportunity to understand the detailed timescale of magmatic evolution. We discuss the timescale of chemical evolution in the Utsubo granitic pluton using precise U-Pb zircon geochronology, zircon oxygen isotope analysis, and the Ti-in-zircon thermometer.

The Utsubo granitic pluton is situated in the Hida belt, the northernmost geotectonic unit in the Inner Zone of the Southwest Japan Arc. The calc-alkaline plutons in the Hida belt have been divided into two types based on petrology and Sr and Nd isotopic ratios; Type-1 has a limited range in initial Sr and Nd isotopic values, and Type-2 has a wider range (Arakawa and Shinmura, 1995).

The Utsubo granitic pluton, emplaced into the Hida gneiss, is a Type-1 pluton with normal lateral compositional zoning: tonalite, granodiorite, pink coarse-grained granite, and fine-grained granite from its margin to center (Kano, 1990).

2. Results and Discussion

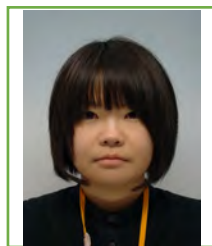
Zircons extracted from tonalite, granodiorite, and coarse-grained granite yielded 192.2 ± 1.4 , 190.0 ± 1.3 , and 188.5 ± 1.4 Ma. The results indicate that the time interval from tonalite to coarse-grained granite is 3.7 ± 2.0 Ma.

The mean oxygen isotope ratios ($\delta^{18}\text{O}_{\text{VSMOW}}$) in zircons decrease by about 0.54‰ for about a 12% increase in SiO_2 , tonalite to granite. The calculated whole rock $\delta^{18}\text{O}$ on the correlation between $\Delta^{18}\text{O}_{(\text{WR-zircon})}$ and silica content ($\Delta^{18}\text{O}_{(\text{WR-zircon})} = 0.0612\text{SiO}_2 - 2.50$; Lackey et al., 2008) is 7.81 ‰ (tonalite), 8.13 ‰ (granodiorite), 8.05 ‰ (granite), using the SiO_2 contents measured by Arakawa and Shinmura (1995). Closed-system differentiation of mafic magmas typically produces an increase in whole-rock $\delta^{18}\text{O}$ of about 0.5‰ for each 10% increase in SiO_2 (Taylor & Sheppard, 1986). Lackey et al. (2008) reported that the whole-rock $\delta^{18}\text{O}$ of calc-alkaline systems (the Tuolumne suite) increases by about 1.0‰ for each 10% increase in SiO_2 , while the $\delta^{18}\text{O}$ of the zircons is relatively constant.

The zircon crystallization temperatures were calculated from the Ti content of zircon using the equations of Watson et al. (2006) and Fu et al. (2008). The Utsubo granitic rocks contain zircon and titanite (CaTiSiO_5). The TiO_2 activity of the Utsubo granitic melt is unknown. However, it can be assumed to range from about 0.6 to 0.9 because zircon was saturated in this melt, and rutile is not observed. The zircon crystallization temperatures were calculated assuming TiO_2 activity is 0.7. The mean zircon crystallization temperature of the Utsubo granitic rocks is constant. On the other hand, the zircon saturation temperatures calculated by the methods of Watson & Harrison (1983) increase with increasing SiO_2 . Bulk rock compositions of SiO_2 , Al_2O_3 , Na_2O , CaO , K_2O , and Zr were obtained from Arakawa & Shinmura (1995). The zircon saturation temperature of the Utsubo granitic rocks increases from about 730 to 790°C with the increase in SiO_2 .

References

- Arakawa, Y., Shinmura, T. (1995) Nd-Sr isotopic and geochemical characteristics of two contrasting types of calc-alkaline plutons in the Hida belt, Japan. *Chemical Geology*, 124, 217-232.
- Kano, T. (1990) Granitic rocks in the Hida complex, central Japan. *Mining Geology*, 40, 397-413.
- Lackey, JS, Valley, JW, Chen, JH, Stockli, DF. (2008) Dynamic Magma Systems, Crustal Recycling, and Alteration in the Central Sierra Nevada Batholith: the Oxygen Isotope Record, *Journal of Petrology*, 49, 1397-1426.
- Taylor, HP, Sheppard, SM. (1986) Igneous rocks; I, Processes of isotopic fractionation and isotope systematics. *Reviews in Mineralogy and Geochemistry*, 16, 227-271.
- Watson, EB, Wark, DA, Thomas, JB. (2006) Crystallization thermometers for zircon and rutile. *Contributions to Mineralogy and Petrology*, 151, 413-433.
- Fu, B, Page, FZ, Cavosie, AJ, Fournelle, J, Kita, NT, Lackey, JS, Valley, JW. (2008) Ti-in-zircon thermometry: applications and limitations. *Contributions to Mineralogy and Petrology*, 156, 197-215.
- Watson, EB, Harrison, TM. (1983) Zircon saturation revisited: temperature and composition effects in a variety of crustal magma types. *Earth and Planetary Science Letters*, 64, 295-304.



Evidence for early ecosystem preserved in banded iron formation of the Isua Supracrustal Belt

Hikaru Tanabe^{1*}, Yusuke Sawaki¹, Masahiro Kayama¹, Yuki Ishihara¹, Tsuyoshi Komiya¹

1. Department of Earth Science and Astronomy, Graduate School of Arts and Sciences, The University of Tokyo, Tokyo 153-8902, Japan.

*corresponding author: h-tanabe2023@g.ecc.u-tokyo.ac.jp

1. Introduction

Previous studies have reported traces of early life in the 3.8 Ga Isua Supracrustal Belt (ISB), southern West Greenland: very low $\delta^{13}\text{C}$ values (e.g. Rosing, 1999) and nano-structures (Ohtomo et al., 2014) of carbonaceous materials in metasedimentary rocks. Furthermore, high $\delta^{56}\text{Fe}$ values of sulfides up to +2.35‰ and low $\delta^{56}\text{Fe}$ values down to -2.41‰ suggest iron-oxidizing bacteria and microbial dissimilatory iron reduction in the Eoarchean, respectively (Yoshiya et al., 2015).

Formation of ecosystem plays an important role on not only evolution of life but also atmospheric evolution. For example, model calculation suggests that presence of only methanogens did not cause methane haze, but presence of phototrophic iron-oxidizing bacteria and methanogens resulted in methane haze (Watanabe et al., 2021). Therefore, it is quite important to investigate the early ecosystem in the Eoarchean, but it is still ambiguous whether other microorganisms inhabited in the Eoarchean.

2. Result

ISB is located in approximately 150 km northeast of Nuuk, Greenland, and is a part of the Itsaq Gneiss Complex. It consists of metasedimentary rocks of clastic sedimentary rocks, chert, carbonate rocks and BIF, as well as basaltic and ultramafic rocks. The northeastern part is divided into three Units: Northern, Middle, and Southern Units, based on the metamorphic grades (Komiya et al., 1999). We collected BIFs in the Northern and Southern Units.

We found carbonaceous material grains in a BIF sample. They comprise mainly disordered graphite because two bands at 1355 (D1-band) and 1582 (D2-band) cm^{-1} are present on their Raman spectra. They are classified into two types based on their occurrence: Inclusions within quartz or magnetite grains, respectively.

Forty pyrite grains with obvious bands at 342, 377, and 428 cm^{-1} on their Raman spectra were found in five BIFs. They are also classified into two types: (1) subhedral–euhedral (square or hexagon) pyrite within goethite grains in quartz-rich bands in three BIFs from the Northern Unit, and (2) small (< 20 μm) rounded pyrite within magnetite grains in two BIFs from the Southern Unit, respectively.

3. Discussion

We estimated crystallization temperature of one of the carbonaceous materials using the Raman spectrum in order to find carbonaceous materials formed before metamorphism. According to a calculation formula (Kouketsu et al., 2014), the crystallization temperature of carbonaceous material is estimated at ca. 150–280 °C, lower than metamorphic grade in this area. The difference is possibly why the carbonaceous material was deformed during making the thin section.

It is considered that the subhedral to euhedral pyrite grains were recrystallized or formed in late diagenesis. Furthermore, the goethite associated with pyrite was probably formed from pyrite under oxic condition during later metamorphism. The rounded sulfide grains may be of early diagenetic or detrital origin.

We will measure sulfur isotopic compositions ($\delta^{34}\text{S}$) of the sulfides and carbon isotopic ($\delta^{13}\text{C}$) compositions of the carbonaceous materials in order to estimate their origins and reconstruct the ecosystem in the Eoarchean.

References

- Komiya, T., Maruyama, S., Masuda, T., Nohda, S., Hayashi, M., & Okamoto, K., (1999) Plate tectonics at 3.8–3.7 Ga: Field evidence from the Isua accretionary complex, southern West Greenland. *Journal of Geology* 107, 515–554.
- Kouketsu, Y., Mizukami, T., Mori, H., Endo, S., Aoya, M., Hara, H., Nakamura, D., & Wallis, S., (2014) A new approach to develop the Raman carbonaceous material geothermometer for low-grade metamorphism using peak width. *Island Arc* 23, 33–50
- Ohtomo, Y., Kakegawa, T., Ishida, A., Nagase, T., & Rosing, M.T. (2014) Evidence for biogenic graphite in early Archaean Isua metasedimentary rocks. *Nature Geoscience* 7, 25–28.
- Rosing, M.T. (1999) ^{13}C -depleted carbon microparticles in > 3700-Ma sea-floor sedimentary rocks from West Greenland. *Science* 283, 674–676.
- Yoshiya, K., Sawaki, Y., Hirata, T., Maruyama, S., & Komiya, T. (2015) In-situ iron isotope analysis of pyrites in ~3.7 Ga sedimentary protoliths from the Isua supracrustal belt, southern West Greenland. *Chemical Geology* 401, 126–139.
- Watanabe, Y., Tajika, E., Ozaki, K., Hong, P.K. (2021) Haze Formation Limits the Primary Productivity of Marine Anaerobic Ecosystem during the Archean, *Goldschmidt Conference 2021 Virtual*.



DEFORMATION PATTERNS OF AN ACCRETIONARY PRISM REVEALED BY SANDBOX EXPERIMENTS

Satoshi Tonai¹, Motoharu Tsuboi¹, and Takami Tachibana¹

1. Faculty of Science and Technology, Kochi University, Japan
s-tonai@kochi-u.ac.jp

1. Introduction

Some shallow slow earthquakes observed at the plate boundary are thought to occur within the subduction wedge (e.g., Ito and Obara, 2006). Therefore, it is important to understand the deformation processes that occurs inside the tip of the wedge to establish the mechanism of shallow slow earthquakes. In this study, we constructed a Coulomb wedge in analogue (sand box) experiments using dry sand (Toyoura silica sand) and analyzed images of the developed wedge using digital image correlation (DIC). In particular, we traced shear bands such as the backthrust (BT), a forward-dipping fault at the rear of the wedge, and the frontal thrust (FT), a backward-dipping fault at the tip of the wedge. At the same time, load measurement was carried out using a load cell to explore how much the BT contributes to intra-wedge deformation.

2. Method

The experimental method was as follows. An adhesive sheet was placed inside an acrylic box with a load cell and an actuator. A 16-mm-thick layer of Toyoura sand covered the bottom of the box, and a camera was placed next to the sand layer. The actuator was pulled over a distance of 250 mm at a velocity of 0.4 mm/s to create a wedge. Up to 500 images were obtained at an interval of 1 image every 0.4 mm of sheet movement over a displacement of 50–250 mm. The obtained images were imported into a PC and analyzed using DIC. The linear region with a principal strain of >1.0% and located close to the fixed wall was identified as the BT, and the distance from the intersection of the BT and FT to the fixed wall was measured. Results were compared with load data to investigate the correlation between the location of the BT and the load.

3. Results

As a result of the experiment, it was clarified that the timing and place of formation of FT and BT changed depending on filling rate of sand layer. The high-filling-rate layer (filling rate of about 67%) has fewer shear bands, the displacement period of one shear band is longer, and the shear bands. It was concluded that these characteristics are caused by the degree of strain weakening during the formation of shear bands. In addition, it was found from the experiment that the

displacement of the BT greatly contributed to the deformation within the wedge. The displacement of the FT is large, but it is accumulated when the FT is formed at the wedge tip. The FT does not displace much when the next FT newly occurs and is positioned inside the wedge. In the low-filling-rate layer experiment, it was clarified that the deformation inside the wedge was not localized but occurred over a wide area of the wedge.

4. Discussion

Based on the scaling law (e.g., Lohrmann et al., 2003; Schellart and Strak, 2016), the deformation discussed in the DIC analysis in this study corresponds to the deformation process every 190–420 years within the several km at the tip of the natural accretionary complex. there is a spatial and temporal gap between analogue experiments and observational data. Thus, improving the resolution of each experiment, analysis, and observation and accumulating data are future tasks to improve the comparison between the analogue experiments and the prototypes.

References

- Ito, Y. and Obara, K. (2006) Dynamic deformation of the accretionary prism excites very low frequency earthquakes. *Geophysical Research Letters*, **33**, L02311.
- Lohrmann, J., Kukowski, N., Adam, J., and Oncken, O., 2003, The impact of analog material properties on the geometry, kinematics, and dynamics of convergent sand wedges. *Journal of Structural Geology*, **25**, 1691-1711.
- Schellart, W. P. and Strak, V., 2016, A review of analogue modelling of geodynamic processes: Approaches, scaling, materials and quantification, with an application to subduction experiments. *Journal of Geodynamics*, **100**, 7-32,

Reconstruction of hydrothermal oceanic chert and banded iron formation in Archean by mineral identification in Pilbara terrane, Western Australia

Yusuke Inokuchi¹, Shoichi Kiyokawa¹

1. Kyushu University, Japan

Banded Iron Formation (BIF) formed by oxidation has been reported at many locations, and there is much debate as to its origin, since in many cases the structure and composition of the deposit was lost due to diagenesis and metamorphic processes. (Holland 2006, Konhauser et al. 2002). For example (1) Fe²⁺ and SiO₂ are supplied from hydrothermal vents and precipitate as divalent iron minerals (siderite (FeCO₃), greenalite (Fe₂₋₃Si₂O₅(OH)₄), greenrust (Fe²⁺₄Fe³⁺₂(OH)₁₂CO₃²⁻·2H₂O), etc.) in the zone deeper than the photic layer. (2) In the photic layer, Fe²⁺ is oxidized by cyanobacteria and precipitated as ferrihydrite (Fe(OH)₃). Then, this ferrihydrite is reduced from Fe³⁺ to Fe²⁺ by the action of methane-reducing bacteria on the seafloor and re-precipitated as siderite, which are models. For primary iron minerals in the BIF, assuming that amorphous silica in seawater at the time was saturated, with greenalite as the primary mineral, four patterns of precipitation models have been proposed (Johnson, 2018). (1) Fe²⁺ becomes saturated in seawater, associates with silica, and precipitates. (2) Fe²⁺ in the water is catalytically oxidized by biological activity or ultraviolet light, and precipitated as (Fe²⁺, Fe³⁺)greenalite. (3) Oxidation of Fe²⁺ generates greenrust, a metastable mineral, which is replaced by low Fe³⁺ greenalite during precipitation and precipitated. (4) Oxidation of Fe²⁺ produces ferrihydrite as a precursor, which is reduced again by iron-oxidizing bacteria and precipitated as low Fe³⁺ type greenalite.

(Stratigraphy) Dixon Island Formation (DX Fm) and Cleaverville Formation (CL Fm) in the Pilbara Coastal Greenstone Belt, Western Australia including well preserved continuous stratigraphic sequence at Mesoarchean oceanic sedimentary section with hydrothermal chert and Iron formation (Kiyokawa et al, 2002). The DX Fm can reconstruct hydrothermal activity 3.2 billion years ago when it transitioned from silicified volcanic rocks to chert (Kiyokawa et al, 2006, Kiyokawa et al, 2019). This formation has a total thickness of more than 400 m, and is composed of three subgroups: The Komatiite-Rhyolite Tuff Member (<250 m thick), the Black Chert Member (7-20 m thick), and the Varicolored Tuff Member (<250 m thick). The CL Fm preserves the 3.1-billion-year-old succession of the transition from black shale to BIF. CL Fm is composed of Black Shale Member and BIF Member. These formations are the least metamorphosed of the BIF Formation and

hydrothermal cherts in Mesoarchean, and are likely to have preserved the stratigraphic information at that time.

(Methods) We used samples from shoreline outcrop of the Black Chert Member of the DX Fm and the CL3 drill core of CL Fm, Iron ore of Brockman Iron Formation were used for detailed observation and analysis to identify the minerals remaining in the rocks. The DX and CL3 samples were thinned and observed by microscopy, SEM, and in some cases by TEM.

(Results) SEM observation of the DX Fm revealed that pyrite is concentrated and arranged as layers, and Apatite crystals were found in the black chert layer just above the Biomat layer. TEM observation of the chert in CL Fm revealed strips of crystals similar to those of greenalite. The apatite in the chert of the DX Formation suggests the possibility of life in a hydrothermal environment, which is consistent with the biomat fossils in the formation and bacterial micro fossil (Kiyokawa et al. 2006). It is possible that this formation preserves information about the early sedimentary period.

References

- Kiyokawa et al., 2002, Structural evolution of the middle Archean coastal Pilbara terrane, Western Australia: *Tectonics*, v. 21, no. 5, p. 8-1-8-24.
- Kiyokawa et al. 2006, Middle Archean volcano-hydrothermal sequence: Bacterial microfossilbearing 3.2 Ga Dixon Island Formation, coastal Pilbara terrane, Australia, *GSA Bulletin*; January/February 2006; v. 118; no. 1/2; p. 3-22
- Kiyokawa et al., 2019, Timing and development of sedimentation of the Cleaverville Formation and a post-accretion pull-apart system in the Cleaverville area, coastal Pilbara Terrane, Pilbara, Western Australia, *Island Arc*; 2019;28:e12324.
- Holland, H.D., 2006. The oxygenation of the atmosphere and oceans, *Philos Trans R Soc Lond B Biol Sci.* 2006 Jun 29; 361(1470): 903-915.
- Konhauser et al., 2002. Could bacteria have formed the Precambrian banded iron formations? *Geology* 30, 1079-1082.
- Johnson et al., 2018, Low-Fe³⁺ greenalite was a primary mineral from Neoproterozoic oceans. *Geophys Res Lett* 45.

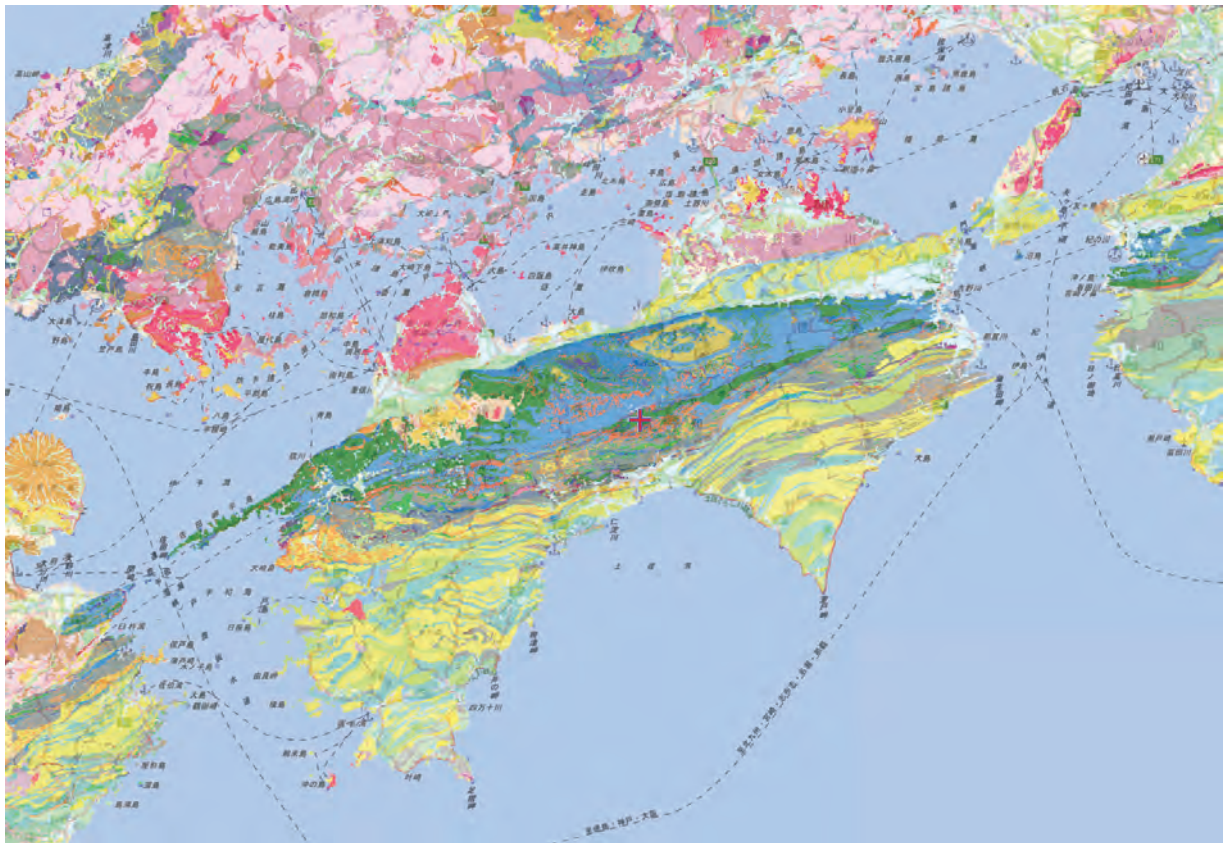


Tatsukushi (Kochi)



Kankakei, Shodoshima Island (Kagawa)

International **WHEEL** seminar _____ 5th IGS
ee| **Precambrian**
World 2023
 Kochi core center* Japan



Seamless geologic map by Geological Survey of Japan (AIST)



National Museum of Nature and Science (geology)
 National Institute of Polar Research (SHRIMP Lab)

